The Thesis Committee for Alan Lee Viosca
Certifies that this is the approved version of the following thesis:

A Method for the Characterization of White Spots in Vacuum-Arc Remelted Superalloys

APPROVED BY
SUPERVISING COMMITTEE:

Supervisor:

Eric M. Taleff

Joseph J. Beaman

A Method for the Characterization of White Spots in Vacuum-Arc Remelted Superalloys

by

Alan Lee Viosca, B.S.M.E.

Thesis

Presented to the Faculty of the Graduate School of

The University of Texas at Austin

in Partial Fulfillment

of the Requirements

for the Degree of

Master of Science in Engineering

The University of Texas at Austin

December 2011

Acknowledgements

I would like to thank Dr. Eric M. Taleff for his patience and guidance through the research and writing process. I would also like to thank Dr. Trevor J. Watt and Dr. Joseph J. Beaman for their assistance with editing and revising this paper. In addition, I owe much thanks to the Special Metals Processing Consortium for their support.

Abstract

A Method for the Characterization of White Spots in Vacuum-Arc Remelted Superalloys

Alan Lee Viosca, M.S.E.

The University of Texas at Austin, 2011

Supervisor: Eric M. Taleff

Vacuum-Arc Remelting (VAR) is an important process for manufacturing Ti- and Ni-based superalloys. Currently, the sources and mechanisms behind microstructural anomalies produced in VAR superalloy ingots are not well understood. In order to help understand formation processes, a method of characterizing specific anomalies in VAR ingots is desired. This paper presents a method of characterizing the composition and morphology of anomalies in VAR alloy ingots using a combination of serial sectioning and X-ray fluorescence (XRF) energy dispersive spectroscopy (EDS) techniques. This process is demonstrated on a dirty white spot from an Alloy 718 sample. The white spot of interest was serial polished and 2-D XRF EDS maps were acquired at each polish depth. The EDS maps were then stacked to form a 3-D representation of the white spot. In addition, SEM and optical microscopy techniques were used to further characterize the composition and morphology of the dirty white spot. The dirty white

spot is composed of both Ti-enriched and Nb-depleted regions. The 2-D EDS maps acquired with the XRF equipment provided adequate contrast for creating a 3-D representation of the Ti-rich region of the dirty white spot. However, contrast was not sufficient to create a 3-D representation of the Nb-depleted region. The XRF EDS equipment combined with SEM and optical microscopy techniques provided valuable information about the morphology and composition of the Alloy 718 dirty white spot. It is concluded that this dirty white spot was produced by fall-in from either the crown or shelf regions during the VAR process.

Table of Contents

List of Tables

List of Figures

Chapter 1: Introduction

1.1 Problem Statement and Research Goals

Vacuum-arc remelting (VAR) is a process of critical importance to the commercial production of special metal and alloys, including nickel-based superalloys and various titanium alloys. The VAR process can produce undesired microstructural features that are not easily removed by subsequent heat treatments or deformation processing. These features may adversely affect the service lives of parts subjected to demanding conditions, such as the high temperatures and cyclic fatigue stresses typical for components made of special metals and alloys. The sources and specific mechanisms behind the formation of these microstructural features are not fully understood. More data are needed to advance the understanding of these and to learn how to prevent undesirable features from forming. The purpose of the present study is to create new experimental techniques that will provide previously inaccessible information and help better understand the formation mechanisms of specific anomalous microstructural features during the VAR process.

The experimental techniques and initial data produced by this study will enable future research into the VAR process. An important purpose of additional data is to guide the development of new, more accurate models for the formation of microstructure during VAR. Models with greater fidelity will be used to better determine the processing parameters that should be controlled during the VAR process in order to prevent formation of undesirable microstructural features. These models will be used to determine improved processing conditions

for VAR. Eventually, control methods for the manufacture of large, defect-free ingots will be created and implemented.

The goal of the present study is to establish and demonstrate a new experimental technique for characterization of pertinent microstructural features produced during VAR. Three-dimensional (3-D) compositional mapping techniques will be developed and used to accurately characterize microstructural features of specific interest. This type of detailed, 3-D microstructural characterization has not previously been carried out on special metals produced by VAR.

1.2 LITERATURE REVIEW

Vacuum-arc remelting (VAR) is a process used to manufacture highly homogeneous superalloy ingots. Figure 1.1 shows a schematic of the VAR process.

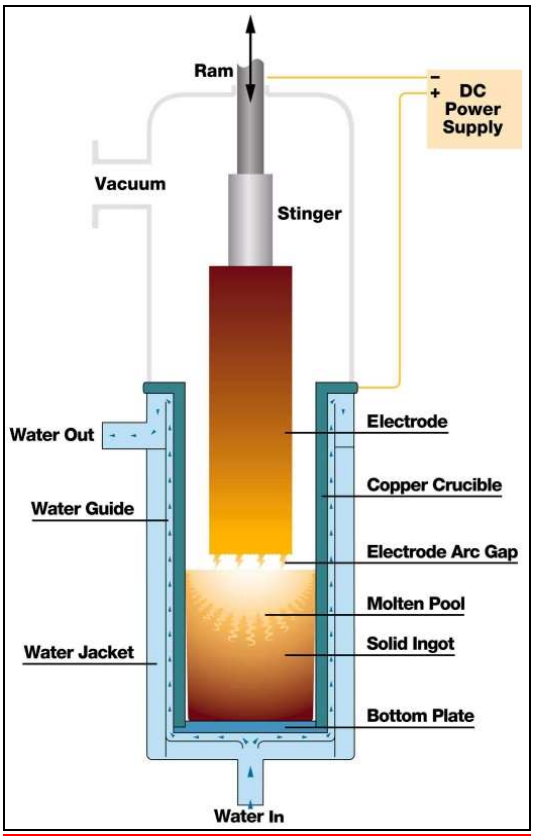

Figure 1.1: VAR Process schematic; figure is from reference [1].

VAR is typically used in the production of nickel- and titanium-based alloys needed for high-temperature applications, especially those involving cyclic fatigue. A small microstructural anomaly in a part manufactured from alloys as these can dramatically reduce service life by acting as an initiation site for fatigue fracture. Current technology limits the maximum ingot size that can be produced without such anomalies. The problems with manufacturing larger anomaly-free ingots are primarily the result of limited understanding of the mechanisms behind defect formation and the resulting inability to predict and control the VAR process to produce defect-free microstructures. In this literature review, the various types of microstructural anomalies are

described. The different compositions and microstructures of undesired microstructural anomalies and their effects on material properties are also described.

1.2.1 Anomaly Nomenclature

Before reviewing the various types of undesirable microstructure anomalies that can be produced during the VAR process, it is useful to note that the most important types are common among most VAR materials. The examples described in this chapter come primarily from investigations of the nickel-based Inconel™ Alloy 718, designation NiCr19Fe18Nb5Mo3Ti1AlCo, UNS# N07718. Table 1.1 shows the amount of major elements in Alloy 718 [2].

Table 1.1: Chemical Composition of Inconel™ Alloy 718 (wt%) [2]

Ni	Cr	Ti	Fe	Nb+ Ta	Mo	Si	Al	Mg	Cu
55.0-55.0	17.0-21.0	0.3-1.3	Bal.	4.50-5.75	2.8-3.3	0.75	0.20-1.0	0.50	0.75

There are two primary types of microstructural anomalies common in Alloy 718 and other superalloys produced through VAR. These are *freckles* and *white spots*. These names originate from their appearance in polished, macro-etched ingots. Freckles are solute-rich regions, which usually appear darker than the bulk material. In titanium alloys, freckles are referred to as *beta-fleck* [3]. White spots, on the other hand, are solute-lean regions, which usually appear as light regions in the macro-etched ingot [4]. The formation of freckles is discussed first, followed by a discussion of white spots.

1.2.2 Freckles

Characteristics:

Freckles are solute-rich regions, which tend to extend radially, toward the center of the VAR ingot. In Alloy 718, freckles are primarily enriched in Nb and are slightly depleted in Cr. The level of Nb enrichment tends to change from the bottom to the top of the freckle, with the bottom having up to 11.5 wt% Nb and the top having approximately 4.5 wt% Nb [5]. Freckles cannot usually be removed by homogenization or by hot-working [6].

Several mechanisms of freckle formation are proposed in the literature. Because of their radial geometry and the variation in Nb enrichment from the bottom to the top of a freckle, the most likely mechanisms of formation are thought to be interdendritic flow, diffusion and solute redistribution. See Figure 1.2 for a diagram of the different regions of a solidifying VAR ingot; dendrites grow radially toward the center of the ingot. This diagram shows the basic parts of a VAR melt, with possible sources of defects detailed. Freckles are formed in the “mushy zone” of the ingot, which is the region between the completely liquid melt pool and the completely solidified ingot.

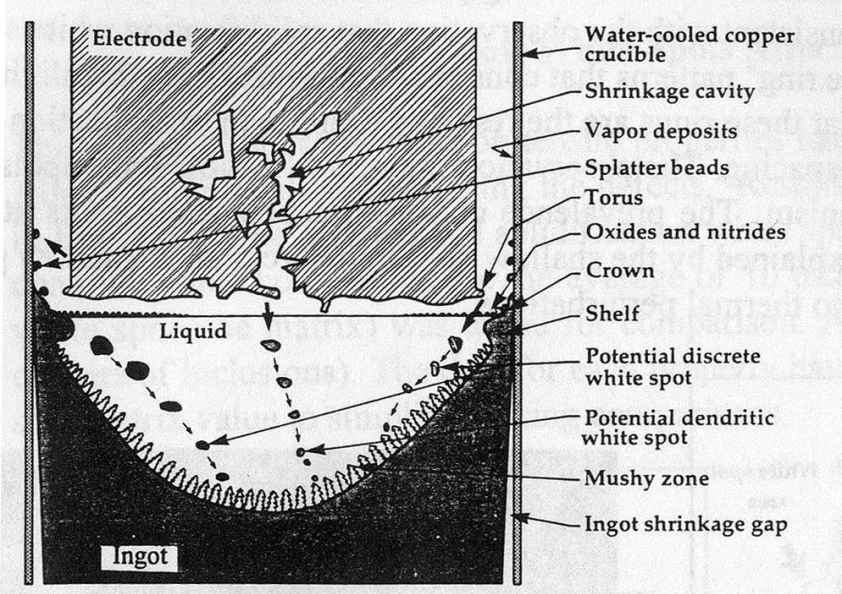

Figure 1.2: Diagram of a solidifying VAR ingot; figure is from reference [4].

A decrease in local melt temperature and local solute enrichment by heavy elements, such as Nb, can cause interdendritic fluid to become denser than the fluid in the molten pool. This produces gravity-driven flow of the interdendritic fluid downward and toward the center of the ingot. As this occurs, dendrites may be dissolved or broken, and a melt fluid channel may form. The shape of these channels will produce the shapes of the freckles by following the curvature of the solidification front [7]. See Figure 1.3 for an illustration of this channeling process. It is believed that the levels of Nb enrichment in Alloy 718 freckles depend on the velocities of the solidus and liquidus isotherms in the melt channel.

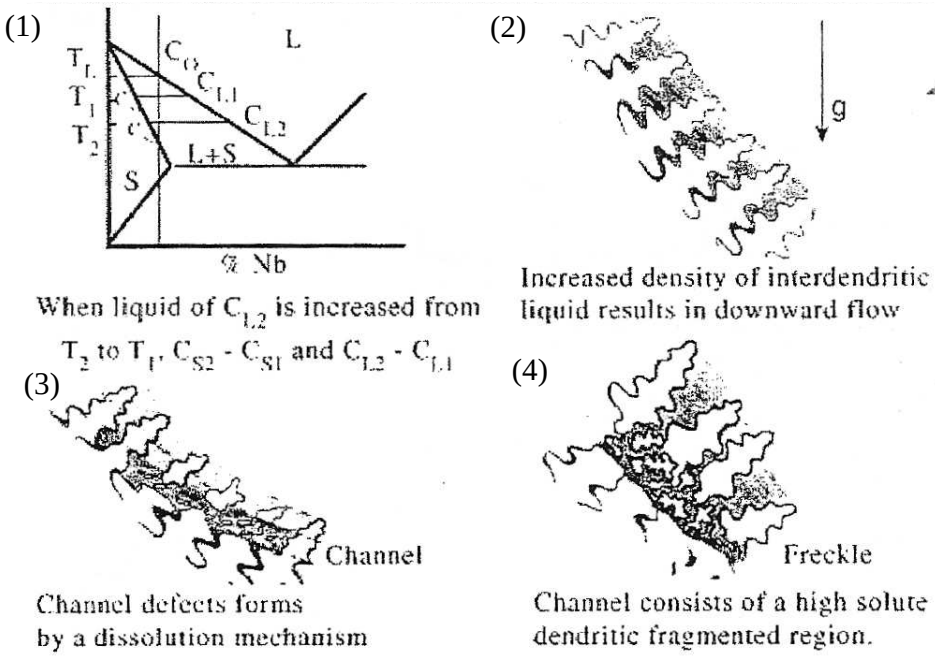

Figure 1.3: An illustration of channel defect formation; figure is from reference [7].

Causes:

All freckles are ultimately caused by large-scale flow behaviors present in the molten regions of the VAR ingot during solidification. Fluids of varying compositions flow in and out of the interdendritic regions as part of these large-scale flows. This can result in macrosegregation and fluid density differences that result in channel defects. Normally, flow in the molten pool is caused by a combination of buoyancy and electromagnetic forces. The buoyancy forces arise from differences in liquid densities, which vary with temperature and composition. The electromagnetic forces come from high currents passing through the melt. Depending on the strength of the current, the buoyancy and electromagnetic forces have different levels of influence over flow in the molten pool [8].

Longer local solidification times give rise to an increased number of freckles [6]. This is because longer solidification times result in more time for diffusion and solute redistribution. Deep molten pools also increase the likelihood of forming channel defects and freckles, due to longer solidification times [7]. It has been shown experimentally that electrode composition has no significant affect on the formation of freckles, as freckles are not inherited from electrodes in VAR processes involving multiple remeltings [8]. Multiple-melt VAR processes use an electrode produced by VAR to produce a subsequent VAR ingot, and this process may be repeated several times, but use is usually limited to “double” or “triple” melts in practice. Each additional melt in the VAR process eliminates undesirable inclusions and produces a more homogeneous final ingot.

Solutions:

Freckles cannot be easily removed from VAR ingots by either deformation processing or heat treating. Freckles must be prevented by adequately controlling the VAR process. In Alloy 718 and most Ni-based superalloys, freckles can usually be prevented by using a short electrode gap and a slow, stable melt rate [6]. Deep molten pools, usually caused by high currents and fast melt rates, contribute to freckle formation because of the slower solidification rates that result [7]. The use of electromagnetic forces to stir the melt pool has become common practice because stirring helps stabilize the electrode arc and drives fluid flow that is beneficial to solidification rates. The level of electromagnetic stirring can be adjusted, along with other control parameters, to prevent freckles from forming [8]. However, white spots may form more easily as VAR conditions are changed to decrease freckle formation.

1.2.3 White Spots

White spots are solute-lean regions that are divided into three types, based on composition, mechanical properties and causes. These are solidification, discrete and dendritic white spots. Solidification white spots are discussed first, because of their similarity to freckle defects.

1.2.3.1 Solidification White Spots

Characteristics:

It is convenient to think of solidification white spots as solute-lean regions that are qualitatively the opposite of freckle defects, which are solute-rich. See Figure 1.4 for an example of solidification white spots in an ingot of Alloy 718.

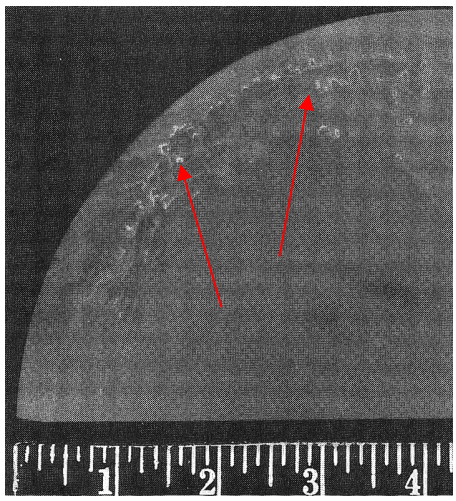

Figure 1.4: Solidification white spots are shown in Alloy 718; image is from reference [4].

Solidification white spots extend radially toward the center of the VAR ingot, as do freckles. However, in Alloy 718, solidification white spots have Nb concentrations ranging from about 4.0 to 5.1 wt% [5]. According to reference [4], no dramatic changes in mechanical properties are associated with the presence of solidification white spots. Solidification white spots are typically on the order of approximately 1000 µm, but vary in size [4]. Just as with freckles, solidification white spots cannot be removed by homogenization or hot deformation.

Mechanisms:

The mechanisms proposed in the literature for formation of solidification white spots are similar to those proposed for freckle formation, and include interdendritic flow, diffusion and solute redistribution [5]. The most significant change from freckle formation is the level of interdendritic flow, which ultimately determines whether a freckle or a solidification white spot is formed. It is believed, as with freckles, that the solidus and liquidus isotherm velocities determine the level of Nb depletion in solidification white spots [5].

Causes:

The causes of solidification white spots are thought to be similar to those of freckle formation. Large-scale flow behaviors in the melt pool produce interdendritic flows, which can cause either enrichment (freckles) or depletion (white spots) of Nb. Thermal perturbations can also cause solidification white spots and, conversely, freckles [4]. An unstable arc can cause melt rates to vary, which can cause solidification white spots.

Solutions:

The best method currently known to prevent solidification white spots is to electromagnetically stir the molten pool. As with freckles, controls can be implemented that essentially eliminate solidification white spot formation during the VAR. Control of the solidus and liquidus isotherm velocities can prevent local Nb enrichment or depletion, the causes of solidification white spots and freckles in Alloy 718. However, there is typically a trade-off, as controls used to prevent white spots can increase the likelihood of freckle formation [5].

1.2.3.2 Dendritic White Spots

Characteristics:

Dendritic white spots, as the name suggests, have a dendritic microstructure. Figure 1.5 shows an example of a dendritic white spot in an Alloy 718 VAR ingot [4].

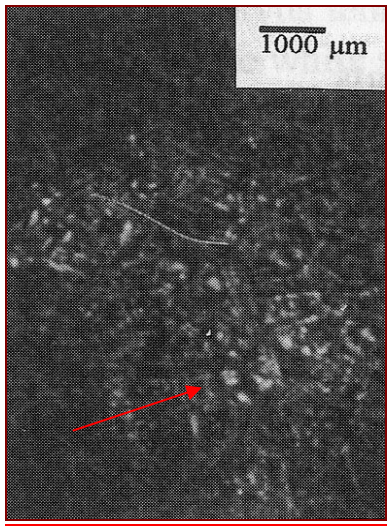

Figure 1.5: A dendritic white spot in Alloy 718; image is from reference [4].

Typically, dendritic white spots are larger than solidification white spots. A typical diameter of a dendritic white spot is around 1500 μm. Nb concentrations in an Alloy 718 dendritic white spot typically range from about 3.8 to 5.1 wt%, similar to solidification white spots. As with other VAR microstructural anomalies, dendritic white spots cannot be removed by subsequent thermo-mechanical treatments [5]. According to reference [4], dendritic white spots do not appear to have a strong effect on strength or fatigue life.

Mechanisms:

Because of the dendritic structure of dendritic white spots in Alloy 718 ingots, it is commonly accepted that these are formed by pieces of the electrode falling into the melt pool during the VAR process [9]. Models have been constructed to simulate the fall-in of a chunk of electrode, and these predict that particles greater than 1.6 to 6.4 mm in diameter typically do not have time to fully melt before sinking to the bottom of the melt pool and forming dendritic white spots [3]. Without sufficient pool superheat, metal may solidify around the detached electrode piece, making it more difficult for the so-called white spot *precursor* to melt before reaching the bottom of the melt pool [9]. During the typical VAR process, it is likely that the electrode breaks many times, detaching small pieces of electrode that drop into the melt pool. However, only the largest pieces become precursors that do not fully melt in the melt pool. These precursors can become dendritic white spots.

Another mechanism has been proposed for the formation of dendritic white spots [5]. This competing mechanism is based upon variations in the composition of melt drips from the electrode and suggests that changing electrode tip geometry and arc behavior can change the composition of these melt drips that fall from the electrode into the molten pool. Because this

mechanism does not explain a dendritic structure in the final ingot, the fall-in mechanism is more likely [5].

Causes:

Electrode fall-in is caused by a combination of initial electrode imperfections and arc instability. If the initial electrode contains a solidification pipe or shrinkage cavity, the pipe may cause fall-in of an electrode piece during the VAR process. During the melting of the electrode, the pipe region within the electrode will tend to melt first, forming a vertical cavity in the center of the electrode. As the metal continues to melt non-uniformly, the arc will become unstable, possibly shorting and moving in a non-continuous pattern across the electrode melt surface. This can cause pieces of the electrode surrounding the pipe cavity to break off and fall into the molten pool. These become dendritic white spot precursors [5, 10]. See Figure 1.6 for a diagram illustrating this process. This mechanism explains the resulting dendritic structure of the defects in the final ingot, which is from the unchanged dendritic structure within the electrode pieces that fall into the melt pool.

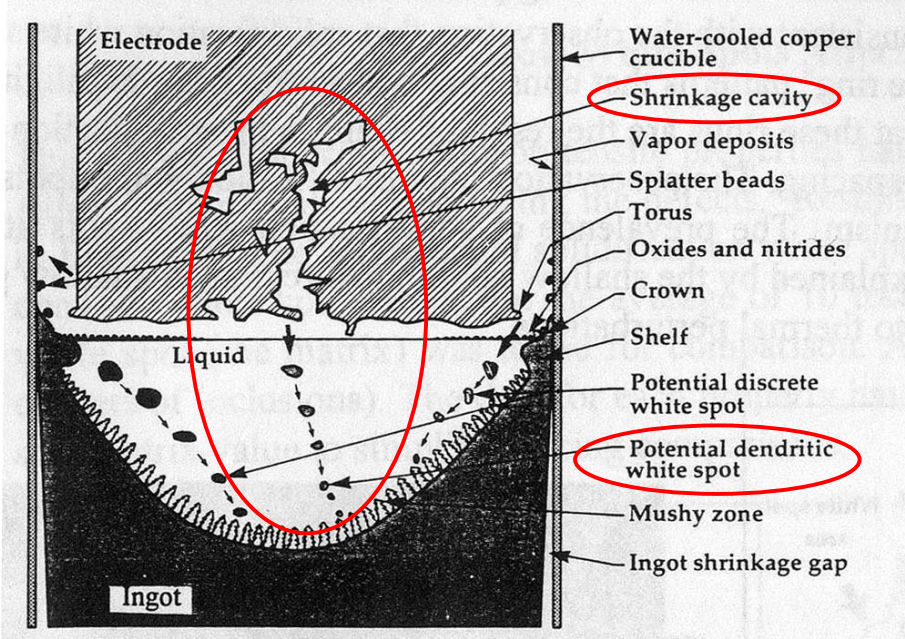

Figure 1.6: Dendritic white spot formation is demonstrated; figure is from reference [4].

Solutions:

The only method known to prevent dendritic white spots is double-melting [10, 11]. Repeating the VAR process makes the ingot more homogeneous, resulting in less piping and more uniform melting of the electrode in the second VAR step. Thus, there are no precursors and no dendritic white spots. In addition, a more uniform electrode makes arc stability easier to achieve [5]. Deeper melt pools can be another solution to this problem, as a deeper melt pool provides more time for the fall-ins to melt. However, a deeper melt pool increases the likelihood of freckle defect formation [7].

1.2.3.3 Discrete White Spots

Characteristics:

The most deleterious of VAR microstructural anomaly is the discrete white spot. Figure 1.7 shows an example of a discrete white spot in Alloy 718.

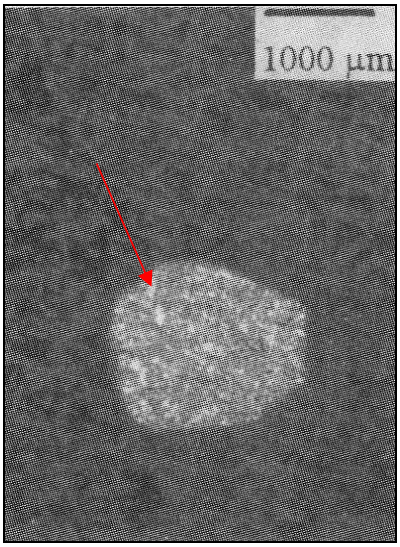

Figure 1.7: A discrete white spot is shown in Alloy 718; image is from reference [4].

Discrete white spots can be classified as *dirty*, those having nonmetallic inclusions, and *clean*, those without inclusions. Discrete white spots in Alloy 718 are usually of sizes similar to dendritic white spots, approximately 1500 µm in diameter, and have Nb concentrations typically ranging from 2.5 to 5.0 wt%. Thus, discrete white spots have the greatest Nb depletion of any type of white spot [1, 10]. Discrete white spots have a greater effect than any other microstructural anomaly on the mechanical properties of Alloy 718 VAR ingots, due to larger concentration differences from the bulk material and a tendency to act as a crack initiation site. According to reference [4], discrete white spots can reduce the yield strength of Alloy 718 by

approximately 27% and can even more dramatically reduce fatigue life. Like the previous defects, discrete white spots cannot be removed by subsequent thermomechanical processing.

Mechanisms:

Discrete white spots in Alloy 718 are caused by material fall-in from the crown, shelf and/or torus regions of the solidifying VAR ingot. See Figure 1.8 for a schematic of discrete white spot formation.

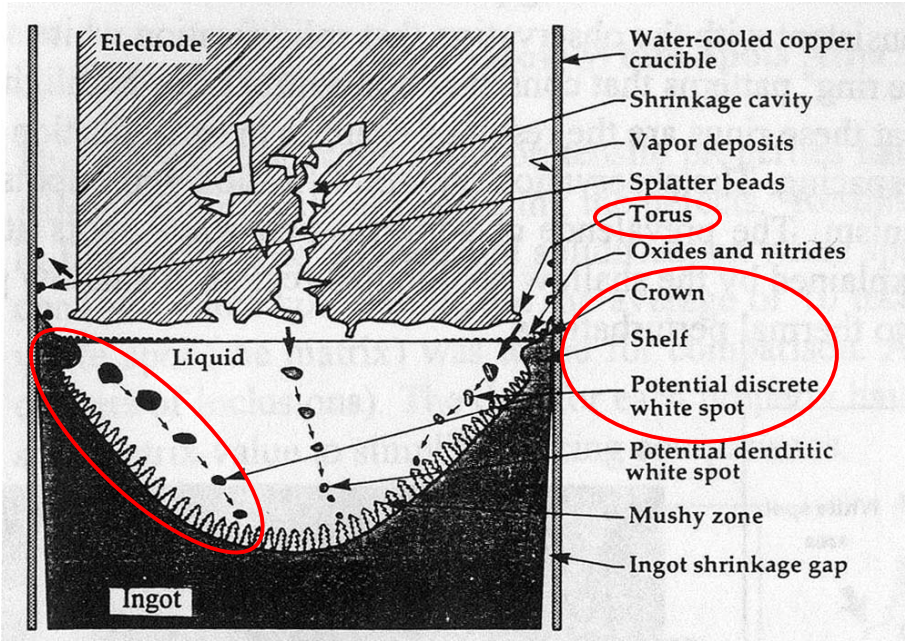

Figure 1.8: Mechanisms of discrete white spot formation are shown; figure is from reference [4].

Compositional analysis supports this formation mechanism, as discrete white spots tend to have the same element concentrations as the crown and shelf [4]. When pieces of the shelf break off, they act as white spot precursors, just as electrode fall-in can form dendritic white spots. If the fall-ins do not spend enough time in the melt pool to fully melt, they will sink to the

bottom of the pool and form discrete white spots. Inclusions, such as oxides, nitrides, and intermetallic compounds, can increase the time required to melt a discrete white spot precursor to significantly beyond that required for a dendritic white spot precursor [4].

Another mechanism proposed for the formation of discrete white spots, similar to the proposed mechanism for dendritic white spot formation, is composition variation from melt drips. Changing electrode tip geometry may change the composition of the material dripping into the molten pool. However, this does not explain the high concentration of inclusions commonly found in discrete white spots [5]. Thus, this second mechanism is considered an unlikely cause of discrete white spots, as it was also considered unlikely for dendritic white spots.

Causes:

The causes of crown, shelf or torus material falling into the molten pool, and ultimately forming discrete white spots, are almost certainly related to flow in the melt pool [4]. Flow, particularly turbulent flow, within the melt pool can cause melting and remelting of the crown and shelf regions, and material is bound to break off and fall into the melt pool during this process. Turbulent flow can result from buoyancy forces, electromagnetic stirring or arc stability [5]. Arc stability is a likely suspect because it is very difficult to control and depends on many variables. In addition, any loss of pool superheat, which is largely governed by arc stability, will increase the chance of forming discrete white spots because fewer fall-ins will be melted [12].

Solutions:

Currently, there are no widely accepted techniques for preventing the formation of discrete white spots. In order to prevent dirty discrete white spots, Alloy 718 electrode material

can be degassed or decarburized to remove the inclusions that ultimately build up in the shelf region [11, 13]. Yet, this is expensive, often impractical and does not solve the problem of clean discrete white spots. A potentially better approach is to stabilize the arc. This can be accomplished by double melting, thus improving electrode homogeneity, or changing arc power levels.

There are two stable arc configurations during VAR. One is a constricted arc, which rotates around the electrode tip while melting it. The other is a diffuse arc, which stays in the center of the electrode and melts it more uniformly [3]. It has been shown that a constricted arc tends to melt the shelf region more and decrease depth of the melt pool. This is because the circular motion of the arc increases pool turbulence. A constricted arc is less efficient at melting the electrode than a diffuse arc [5]. A diffuse arc is preferred to prevent discrete white spots, because the melt pool will be deeper. However, deeper molten pools and higher melt rates may increase the chances of freckle formation [7].

1.3 THREE-DIMENSIONAL MICROSTRUCTURE CHARACTERIZATION

3-D, rather than just 2-D, microstructure characterization is important because of the extra insight that the 3-D data sets give into feature characteristics. 3-D data sets allow for quantitative analysis of variables such as connectivity and adjacency. Brian Chang's work on aluminum alloy AA5083 is an example of the benefits of 3-D characterization over 2-D techniques [14]: With the use of 3-D data sets, cavitation damage produced in AA5083 alloy sheet during deformation by solute-drag creep, which involved elevated temperatures and slow tensile straining, were correlated to specific intermetallic particles in the microstructure. With 2-D data sets, no direct quantitative conclusions could be made as to whether or not these cavities always formed next to particular types of intermetallic particles.

Characterization of Alloy 718 anomalies in 3-D is of increasing importance due to the fact that very little is actually known about their morphologies. 2-D characterization can only provide characterization of composition gradients and morphology in 2-D. With 3-D data sets, composition gradients in all directions can be known, as well as the general shape of the feature in 3-D space. Based on information relating the shape and composition to solidification fronts and ingot faces, 3-D data sets of this type will allow for better inferences into how the anomalies are formed.

1.4 RESEARCH GOALS

The first goal of this study is to develop a new experimental technique for creating 3-D compositional data sets of microstructural anomalies produced in special metals during the VAR process. This method is developed using serial sectioning and X-Ray Fluorescence (XRF) energy dispersive spectroscopy (EDS). The second goal of the study is to implement this technique on an actual microstructural anomaly in an Alloy 718 VAR ingot. Alloy 718 is chosen because of the availability of specimens and the large amount of literature already available for the mechanisms of anomaly formation during VAR of this material. A dirty white spot is chosen for investigation because of this anomaly's particularly deleterious effects on products produced from Alloy 718 VAR material. The data sets produced will be provided to research teams involved in modeling and control of the VAR process. It his hoped that these data will lead to a better understanding of the physics of the VAR process and, thus, to better physics-based modeling and control of the VAR process.

Chapter 2: Experimental Procedures

2.1 INTRODUCTION

This chapter details the process used to collect 3-D compositional data sets. This process requires serial sectioning and X-ray fluorescence (XRF) energy-dispersive spectroscopy (EDS) techniques. Multiple 2-D XRF EDS scans are made of a feature of interest in sequential layers of material, exposed by serial sectioning. These data layers are then stacked to create a 3-D compositional data set. The data set is then segmented and represented as a 3-D figure to show the morphology of the feature of interest. SEM and optical microscopy are also used to acquire additional data.

A Horiba® XGT-7000™ X-ray fluorescence (XRF) microscope was used to collect the 2-D XRF EDS data. This system uses 10 to 50 keV incident X-rays to excite characteristic X-rays from a specimen, which are detected by a high-purity silicon detector and recorded as photon counts versus energy level. The XGT-7000™ has the capability to collect energy spectra over a large (up to 10 cm by 10 cm) area by rasterizing across multiple positions, with a separate spectrum at each position in this 2-D space. This is desirable because the energy spectra over a 2-D area can be viewed as a digital image (e.g., JPEG format image) representing local elemental composition. The XGT-7000™ was used because it provides accurate 2-D indexing of data with a spatial resolution as small as 10 micrometers.

The serial sectioning process consists of polishing a specimen down by a known distance and collecting 2-D XRF EDS data at specific depths in the specimen. An Allied High Tech® Techprep™ polisher with Multiprep™ polishing head was used to complete the polishing part of

the serial sectioning technique. This polisher has the ability to maintain high levels of parallelism between layers, ensuring accurate 3-D indexing of the multiple layers of 2-D data collected. With accurate indexing in 2-D and 3-D, in addition to the compositional accuracy provided by the XGT-7000™, accurate 3-D compositional data sets can be created.

2.2 SETUP AND INSTRUMENTATION

The experimental techniques developed for acquisition of 3-D microstructure and composition data sets require the following instruments: (1) a Horiba® XGT-7000™ X-ray fluorescence (XRF) microscope with a custom stage mount, (2) a serial polisher with an adjustable polishing head (such as the Allied High Tech® Techprep™ polisher with Multiprep™ polishing head), (3) a custom-designed XRF microscope stage, and (4) custom-designed specimen mounting fixture. Other necessary items include supplies for polishing and grinding, selected specimens for instrument and technique calibration, and a plunge micrometer. The XGT-7000™ XRF microscope, serial polishing instrument, custom XRF microscope stage, and custom specimen mount are shown in Figures 2.1 through 2.4, respectively. The custom XRF microscope stage and specimen mount were created so that the same specimen mount can be used in both the XRF microscope and the serial-polishing instrument, thus facilitating good specimen alignment in both instruments. The following software packages are also required: (1) image editing software capable of creating a panoramic image by stitching together multiple small images and (2) reconstruction software for segmenting and creating 3-D reconstructions [15]. Adobe® Photoshop™ Elements is the photo editing software that was used to create panoramic images in this study. Reconstruct© is the program that was used to create 3-D representations from a series of stacked 2-D images [15].

Figure 2.1: Horiba® XGT-7000™ XRF Microscope.

Figure 2.2: Allied High Tech® Techprep™ polisher with Multiprep™ polishing head.

Top

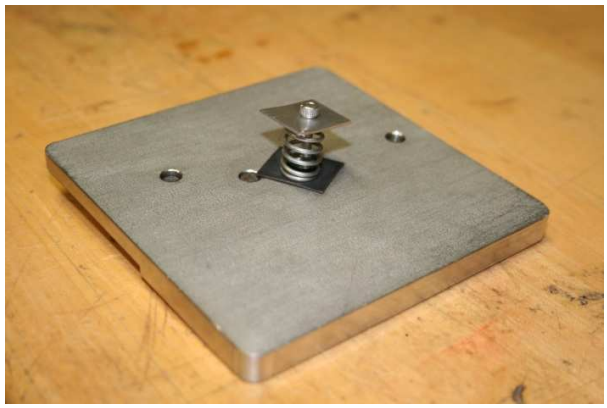

Bottom

Figure 2.3: Custom XRF microscope stage.

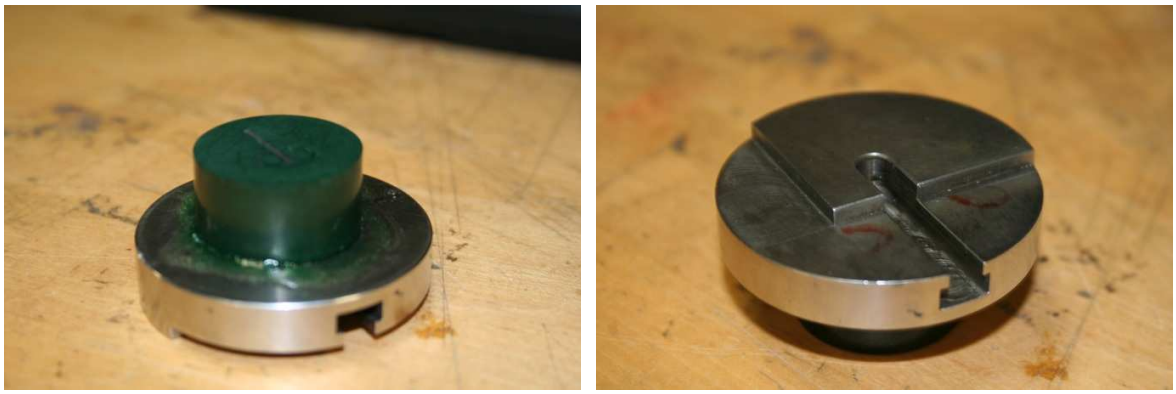

Specimen mounted to top. Bottom side with instrument coupling.

Figure 2.4: Custom specimen mount, with a reference specimen attached; (left) specimen on top and (right) slot for attachment to polishing fixture or XRF microscope stage.

2.3 XGT-7000™ CALIBRATION

A calibration process is used to minimize uncertainties related to the XGT-7000™, and this calibration process should be conducted every few months to ensure that the equipment is not drifting away from proper calibration during normal use. The first calibrations are related to the digital 2-D indexing capabilities of the XGT-7000™ instrument. The applied X-ray position, stage moving distance, and "whole image position" are all variables related to ensuring that accurate 2-D indexing of the EDS data is present throughout the serial sectioning procedure. Without these parameters being calibrated, it is impossible to exactly relate data to position on the specimen. The second set of calibrations is related to the compositional accuracy of the 2-D XRF EDS results. A standard specimen with known composition is scanned and then used to calibrate the software routines used to determine the composition of unknown specimens.

2.3.1 Setting X-Ray Applied Position

Follow the instructions in the Horiba® XGT-7000™ software manual to set the X-ray beam position [16]. This will ensure that the X-rays are actually being applied to the crossing point of the crosshairs in the software image windows.

2.3.2 Compensate Moving Distance

Follow the instructions in the Horiba® XGT-7000™ software manual to calibrate the stage moving distance. This process ensures that the actual distance the stage is moving is consistent with the distance in the optical microscope image.

2.3.3 Calibrate Whole Image Position

Follow the instructions in the Horiba® XGT-7000™ software manual to calibrate the whole image position. This process ensures that the whole image and detail image cameras are displaying the same locations, which is necessary when setting up multiple scans of large areas.

2.3.4 Set Single-Spectrum Standard

This section details how to save a single spectrum from a standard specimen for purposes of comparison to a different specimen of the same type of material. For example, this method can use a spectrum acquired from an Alloy 718 *standard* in order to quantify a *non-standard* Alloy 718 specimen. First, a spectrum from a specimen of known composition must be obtained. Follow the manufacturer's instructions to obtain a single spot scan spectrum under the desired operating conditions [16]. Then, set a single-spectrum standard with the following procedure, starting in the Horiba XGT-7000™ software.

1. In the spectrum analysis window, click “quant.”
2. Click “FPM quant. analysis.”
3. Click “quant. setup.”
4. Choose “quant corr: standard”, and check the “use std. composition” box.
5. Click “standard.”
6. Choose the spectrum from the drop-down menu.
7. Click the “spectrum” tab and choose the elements present.
8. Click the “settings” tab, input each element’s concentration in the appropriate column as reported in the *standard* sample.
9. Click “regist. std.”
10. Click “save”, and save the file with an appropriate name.
11. Click “return.”
12. Click “quant. setup.”
13. Click “file” and choose the standard saved in step 10.

The software will use this standard for all quant. calculations as long as the option “FPM quant. analysis” is selected.

2.4 UNCERTAINTY DETERMINATION

This process is used to create a reference specimen and determine the uncertainties related to the XGT-7000™ two-dimensional stage position. Assuming that the entire custom mounting fixture is rigid and that the specimen/polishing platen interface is rigid, there are three sources of specimen position uncertainty in the 2-D plane of the stage. The first is ΔO.S., or uncertainty related to the origin search performed by the XGT-7000™ software. The second is ΔVac, or uncertainty related to vacuum cycling of the XGT-7000™ between scans. The last is

ΔSpec, or uncertainty related to the interface between the custom XGT-7000™ stage and the custom specimen mount. If these uncertainties are determined to be small relative to the accuracy needed, then it can be assumed that the XGT-7000™ software performs all necessary two-dimensional indexing to sufficient accuracy and that the digital position of the stage given by the software is sufficient. If the uncertainties are large enough to prevent the desired accuracy in position measurement, a modified indexing techniques or redesigned specimen mounting may be necessary. For this study, the position reported by the XGT-7000™ software was of sufficient accuracy to avoid such additional procedures, as is shown in Table 2.1.

2.4.1 Creating a Reference Specimen

A reference specimen can be made from nearly any scrap material. Follow this procedure to create a reference specimen that will be used to quantify the uncertainties in the XGT-7000™ stage position.

1. Section an appropriate piece of material so that it can be placed on the XGT-7000™ stage. Ensure that the top and bottom faces of the specimen are relatively parallel, to avoid any focusing issues in the XGT-7000™. Approximately 1 mm or less variation in specimen thickness is adequate for XRF EDS analysis without focusing issues.
2. Polish the face of the specimen to remove any large surface imperfections. A final polishing grit of 600 is adequate.
3. Place a Vicker's hardness indentation somewhere on the top face of the specimen. The vertex and edges of this hardness indentation will be used to measure the accuracy of the stage position.

For this study, a previously sectioned and mounted penny was used as a reference specimen. The hardness indentation was placed in the Zn interior of the penny, which provided a relatively large indentation due to the softness of the material.

2.4.2 Determining ΔO.S.

1. Place a reference specimen on the custom XGT-7000™ stage and secure it. See Figure 2.5.

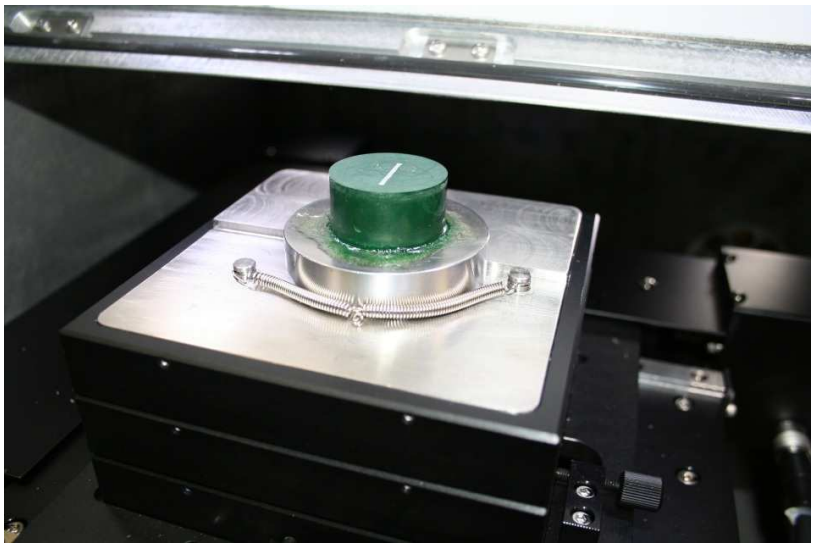

Figure 2.5: Custom stage mount with reference specimen secured.

2. Evacuate the XGT-7000™ specimen chamber.
3. Follow the XGT-7000™ operating procedures to locate the reference feature on the specimen.
4. Capture an optical image and record the stage position.
5. Move the stage around manually, and shut down the XGT-7000™ software, but do not shut down the hardware or vent the chamber.

6. Restart the XGT-7000™ software and perform an origin search.
7. Input the stage position from the first image and acquire a new optical image.
8. Repeat steps 4 through 7 three more times.
9. Using image-editing software, e.g., Photoshop™ Elements, mark a feature of interest on each reference specimen image. Then, overlap the first image with the second, the second with the third, the third with the fourth, and so on. See Figure 2.6 for an example of this process.

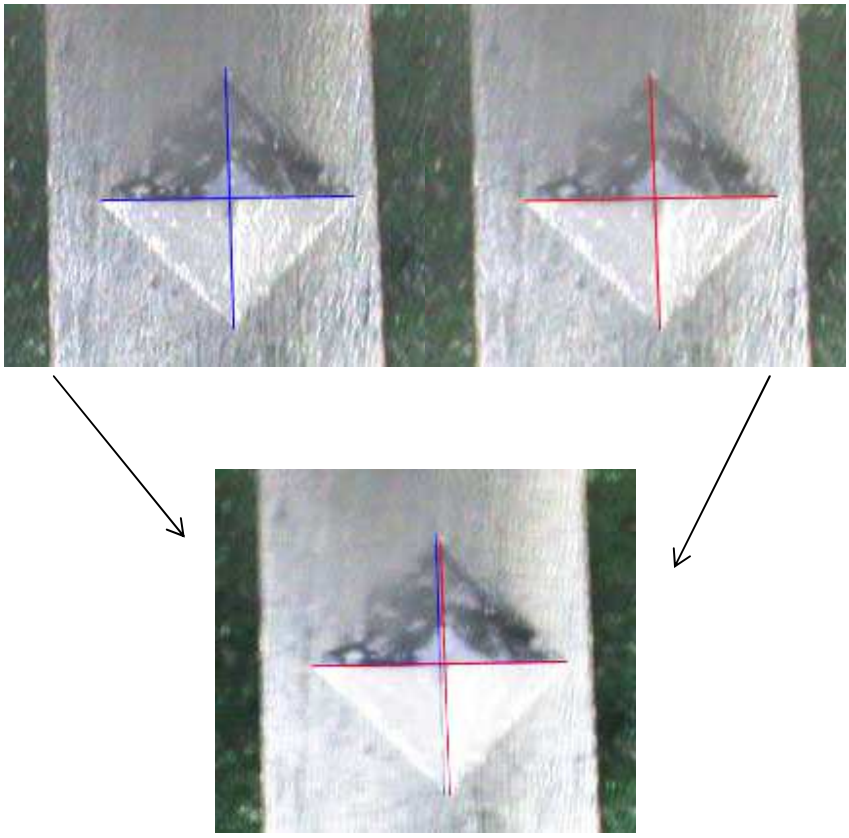

Figure 2.6: Example of marking and overlapping reference specimen images.

10. Measure the x- and y-distance differences between the vertices of the hardness indentations in the consecutive sets of overlapped images obtained in step 9.

11. Average the differences in x- and y- position. The x- and y-averages are used as measures of the uncertainties in the origin search process, ΔO.S.

The value determined for ΔO.S. is provided in Table 2.1.

2.4.3 Determining ΔVac

1. Follow steps 1through 4 in the above procedure, used to determine ΔO.S.
5. Leave the stage in the same position and the software running while venting the XGT-7000™ chamber and then again pumping it down to a vacuum.
6. Acquire another optical image.
7. Repeat steps 5 through 6 three more times.
8. Follow steps 9 through 11 in the procedure used to determine ΔO.S. The x- and y-averages of the offsets are used as measures of the uncertainties related to the vacuuming process, ΔVac.

The value determined for ΔVac is provided in Table 2.1.

2.4.4 Determining ΔSpec

1. Follow steps 1 through 4 in the procedure used to determine ΔO.S.
5. Leave the software and hardware on during the following.
6. Vent the specimen chamber, remove the specimen with its mount, then replace and secure it in the chamber again.
7. Evacuate the chamber and measure the stage position from step 4.
8. Acquire an optical image.
9. Repeat steps 5 through 8 three more times.

10. Follow steps 9 through 11 in the procedure used to determine ΔO.S. The x- and y-averages of the offsets are used as measures of the uncertainties related to the specimen removal and replacement process, ΔSpec.

The value determined for ΔSpec is provided in Table 2.1.

Combine ΔO.S., ΔVac, and ΔSpec using the root-sum-squares (RSS) method [29]. See Table 2.1 for a summary of the uncertainty results from this study.

Table 2.1: Stage Uncertainties (±μm)

	ΔO.S., Avg.	ΔSpec., Avg.	ΔVac., Avg.	ΔTotal, RSS Method
x-direction	6.57	6.38	4.28	10.11
y-direction	5.55	3.29	2.34	6.86

2.5 EDS CHEMICAL COMPOSITION CHARACTERIZATION PROCEDURES

There are two overall stages to the composition characterization process: Data acquisition and data indexing/analysis.

2.5.1 Data Acquisition

The data acquisition part of XRF EDS chemical composition characterization consists of three parts: Specimen mounting, parallel polishing, and XRF EDS data acquisition.

SPECIMEN MOUNTING

1. Section the specimen of interest for mounting. Use appropriate tools, such as an abrasive saw, to section the specimen so that the feature of interest is visible. The sectioned

specimen should not be more than one inch tall and must fit onto the custom polishing mount.

2. Mount the specimen on the custom polishing mount using hot-melt wax or a similar adhesive. Ensure that the feature of interest is facing up.

PARALLEL POLISHING

1. Calibrate the serial polisher according to the manufacturer's instructions [17]. It is most important to calibrate the parallelism between the polishing head and the grinding surface. See Figure 2.7 for an example of the calibration setup. Table 2.2 shows depths polished and levels of specimen parallelism achieved across a distance of 25.4 mm. Levels of specimen parallelism, meaning variation in vertical height of the specimen, above 10 µm/25.4 mm are due to set screws on the serial polisher becoming loose during polishing and affecting polishing head calibration.

Table 2.2: Depths Polished and Parallelism Achieved

Layer	1 to 2	2 to 3	3 to 4	4 to 5	5 to 6	6 to 7	7 to 8
Depth Polished (µm)	49.80	67.40	56.20	50.80	61.80	61.40	62.20
Parallelism * (±µm)	3.11	2.61	2.17	19.40	12.13	3.91	2.05
Layer	8 to 9	9 to 10	10 to 11	11 to 12	12 to 13	13 to 14	
Depth Polished (µm)	50.00	70.80	49.40	63.00	56.40	56.00	
Parallelism * (±µm)	5.83	4.76	4.45	7.21	2.41	3.94	

* Parallelism is measured relative to the width of the sample (25.4 mm).

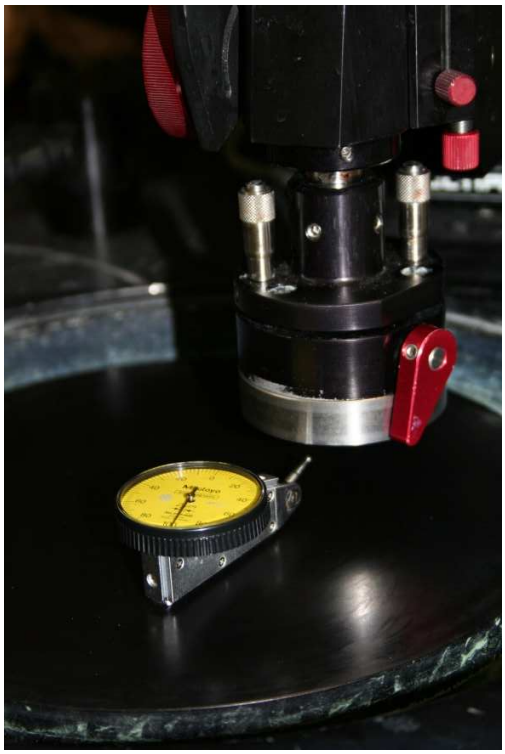

Figure 2.7: Serial polisher set up to calibrate parallelism.

2. Polish the surface of the specimen until it is free of surface irregularities and has a surface roughness sufficiently low for XRF EDS analysis. The XGT-7000™ does not require a very smooth finish. A 600 grit finish is sufficient. Start with rough-grit carbide paper and work gradually to a 600-grit carbide paper. Depending on the type of material being prepared, polishing with a diamond media may be necessary to remove all surface irregularities.
3. Using the plunge micrometer, measure the height of the specimen surface at various locations to ensure a reasonable level of parallelism, or variation in vertical height (± 2 to 5µm). Five measurements at different locations are typically sufficient. Record these values.

4. Follow the procedure for XRF EDS data acquisition (next section) to acquire the first layer of data. Return to step 5 of this section once this layer of data has been acquired.
5. Using Equations (2.1) and (2.2), below, and the bulk composition determined in step 4 of the procedure for acquiring a spot scan data, calculate the X-ray penetration depth for the specimen. Assume that I/I_o is 0.95 for a 95% absorption depth. Example calculations for Alloy 718 are presented in Table 2.3. The penetration depth is used to practically determine the minimum depth that must be removed from a specimen before acquiring the next layer of XRF EDS data.

$$\mu_{TOT} = \sum_i \mu_i w_i$$ Equation (2.1) from reference [18].

where μ_i = mass absorption coefficient of each element present,

and w_i = mass fraction of each element present.

$$x = \frac{\ln(\frac{I}{I_o})}{\mu\rho}$$ Equation (2.2) from reference [18].

where μ = mass absorption coefficient,

ρ = density of material,

and x = depth of penetration.

Table 2.3: Penetration Depth Calculations for Alloy 718				
Element	w_i [19]	μ_i @ 50keV (cm^2/g) [20]	Alloy 718 Parameters	
Ni	0.500	2.078	μ_{TOT} (cm^2/kg)	2.041579
Cr	0.170	1.278	ρ (kg/m^3) [19]	8220
Fe	0.236	1.638	I/I_o	0.95
Nb	0.048	4.884	x (m)	3.05649E-05
Mo	0.028	5.074	x(µm)	30.56487231
Ti	0.007	0.974		
Al	0.002	0.184		
Co	0.010	1.799		

6. Re-calibrate the serial polisher according to the manufacturer's instructions to ensure parallelism.
7. Using the plunge micrometer, once again measure the height of the specimen in five different locations and record these values. DO NOT TURN OFF OR ZERO THE MICROMETER AFTER THIS STEP.
8. Using an appropriate grit abrasive paper, polishing load and polishing time, grind/polish the specimen down to a desired depth, depending on the results of step 5. It is recommended to use a small sample of the bulk material from the specimen to determine an appropriate polishing technique before actually polishing the surface containing the

feature of interest. Doing this will ensure that the proper grit abrasive papers, polishing load, and polishing time are used.

9. Use the plunge micrometer to measure the height of the specimen in the same five locations that were measured in step 7. Record these values.
10. Subtract these values from the values obtained in step 7 and average them all to determine the depth that was polished. Also determine the standard deviation of these values to ensure that a reasonable level of parallelism was achieved.
11. Repeat this process of polishing and XRF EDS data acquisition for as many layers as desired.

XRF EDS DATA ACQUISITION

1. Affix the specimen and its mount onto the custom stage in the XGT-7000™.
2. Evacuate the XGT-7000™ specimen chamber, perform an origin search and acquire an optical image of the whole specimen.
3. If nominal compositions of the feature of interest and bulk regions are desired, move to the next section on acquiring spot scan data. If only 2-D EDS maps are needed, skip to the subsequent section on acquiring 2-D EDS maps.

ACQUIRING SPOT SCAN DATA

1. Click on “acquisition setup.” Choose appropriate settings for voltage, current, and process time. It is recommended that the 400 µm X-ray capillary be used for this step if the feature is not smaller than this diameter. If it is, use the 10 µm X-ray capillary. The larger X-ray capillary provides a stronger signal and better accuracy in composition determination. Voltages available are 10, 30, and 50 keV. Use a value of 50 keV if the

characteristic energy levels of the elements in the specimen span a large energy range. Use a value of 30 keV if the characteristic energy levels do not span such a large range. Use 10 keV if the characteristic energy levels are relatively low. A value of 50 keV is recommended for Alloy 718. Current should be left on auto. The software will adjust the current to compensate for dead time. The larger the process time, the longer a scan will take, but the more accurate the data will be. A process time of 5 to 6 is typically desired. Process time is a unitless parameter.

2. Click on "acquire spectra," and run a single-point scan in order to get a nominal composition for each feature of interest. Run this scan for at least 15 minutes to achieve a reasonable accuracy in subsequent data analysis. Record the spectrum acquired from this single-point scan. If the specimen has multiple locations of interest, run a single-point scan at each location (e.g. if there are multiple microstructural anomalies present).
3. Click on "confirm elements" and choose the elements that are to be used in the quantification of each spot scan.
4. Click on "quant." The results presented here are the quantification results of your spot scan.
5. Move on to the next section, acquiring 2-D XRF EDS maps.

ACQUIRING 2-D XRF EDS MAPS

1. Click on "mapping" and then "Smartmap setup."
2. Choose appropriate settings for voltage, current, and process time. Choose the 10µm X-Ray capillary. Current should be left at 1 mA for 2-D mapping.
3. Click on "Smartmap" and locate a feature of interest.
4. Set "survey time per frame" to a reasonable number, such as 100 to 200 seconds.

5. It is often desired to have a pixel size on the same scale as the X-ray capillary. To achieve this, set up a square around the feature of interest to achieve a pixel size of 10 µm, or slightly less. If the entire feature of interest cannot be encompassed by a single square with this pixel size, move to the section about acquiring a mosaic of multiple 2-D XRF EDS maps. If a mosaic is not necessary, skip to the section on acquiring single 2-D EDS maps.

Acquiring a Mosaic of Multiple 2-D XRF EDS Maps

1. Click on the "multimap" tab and check the "mosaic" box. Set up a grid of squares around the feature of interest, adjusting the x- and y-dimensions of the grid of multiple squares to encompass the entire feature. Ensure that the pixel size is still approximately 10 µm. If it is not, adjust the original square size and cover the desired area by increasing or decreasing the number of squares in the multimap grid. See Figure 2.8.

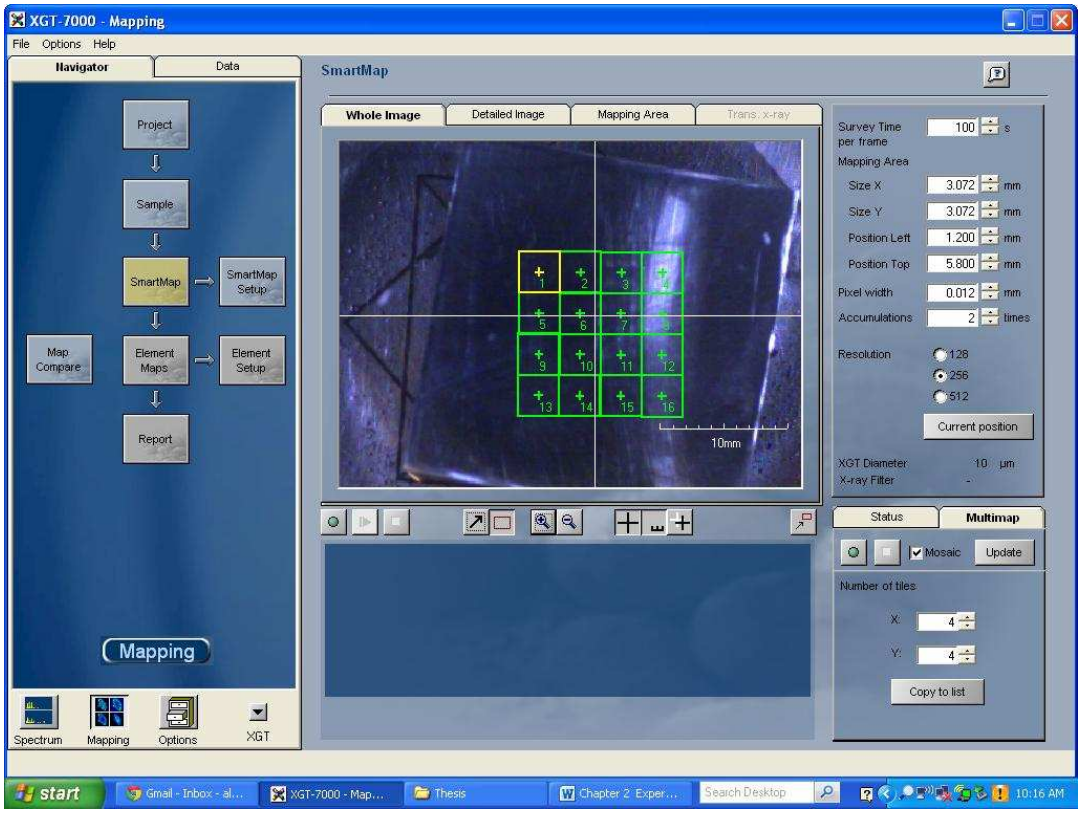

Figure 2.8: An example of a multimap setup [16].

2. Set the number of accumulations as desired. Six accumulations is a reasonable number. The larger the number of accumulations, the higher the contrast between elements will be. If there is a very slight difference in element concentration between the feature of interest and the bulk material, use more accumulations. Be aware that increasing the number of accumulations greatly increases scan time. Set the resolution to a desired level, and record all of the parameters on the screen.
3. Click the green run button that is in the multimap tab.

4. Once the scans are complete, click on the “Confirm Elements” box. (NOTE: Each scanned area will be saved as a separate project, and the following steps are required for each project file for this layer of data.)
5. Either use the “AutoID” function or manually identify elements pertinent to the feature of interest.
6. Click on “Element Maps.”
7. Click the “normalize” button at the top of the screen. This function calculates the minimum and maximum intensity values in the map, and plots all of the data within this range.
8. Right-click on each EDS map that will be used for the 3-D reconstruction and export the images as JPEG files.
9. Remove the specimen from the XGT-7000™, and repeat the parallel polishing and XRF EDS data acquisition procedures for as many layers as needed. Be sure to input the same exact mapping positions and scan conditions as used for the first layer into the XGT-7000™ software. Proper two-dimensional indexing depends on this. Also try to follow the same movements when securing the polishing platen to the mounting stage in order to minimize positioning errors.
10. Once all of the images of each layer of data have been exported from the XGT-7000™ software, it is time to move on to Section 2.5.2, data indexing and analysis.

Acquiring Single 2-D XRF EDS Maps

1. Set the number of accumulations as desired. Six accumulations is a reasonable number. The larger the number of accumulations, the higher the contrast between elements will be. If there is a very slight difference in element concentration between the feature of

interest and the bulk material, use more accumulations. Be aware that increasing the number of accumulations greatly increases scan time. Set the resolution to a desired level, and record all of the parameters on the screen.

2. Click the green run button that is below the image window.
3. Once the scans are complete, click on the “Confirm Elements” box.
4. Either use the “AutoID” function or manually identify elements pertinent to the feature of interest.
5. Click on “Element Maps.”
6. Click the “normalize” button at the top of the screen. This function calculates the minimum and maximum intensity values in the map, and plots all of the data within this range.
7. Right-click on each EDS map that will be used for the 3-D reconstruction and export the images as JPEG files.
8. Remove the specimen from the XGT-7000™, and repeat the parallel polishing and XRF EDS data acquisition procedures for as many layers as needed. Be sure to input the same exact mapping positions and scan conditions as used for the first layer into the XGT-7000™ software. Proper two-dimensional indexing depends on this. Also try to follow the same movements when securing the polishing platen to the mounting stage in order to minimize experimental errors.
9. Once all of the images of each layer of data have been exported from the XGT-7000™ software, it is time to move on to Section 2.5.2, data indexing and analysis.

2.5.2 Data Indexing and Analysis

This procedure consists of two steps: composite image creation (merging) and 3-D reconstruction. If a mosaic of 2-D EDS maps was not necessary, skip to the section on 3-D reconstruction.

COMPOSITE IMAGE CREATION

1. Open Photoshop™ Elements and open all of the JPEG images acquired with the XGT-7000™.
2. Crop the scale bars out of the images, if they are present. This can be accomplished manually for each image or by automating the process. Process automation is only possible in recent versions of Photoshop™ Elements. Ensure that the amount of cropping is the same for each image (not necessary if the process is automated). Save all of the images.
3. If the multimap feature was not used to acquire a series of images for each layer of data, skip to step 9.
4. Click on “file -> create Photomerge.™”
5. Load all EDS images of a particular element’s concentration for layer 1.
6. Arrange the images to create a composite image. There should not be any overlap between the images, and the final image should be the same as the structure of the multimap that was set up on this layer. See Figure 2.8 for an example of the composite image creation process.
7. Click “Ok” and save the composite image.
8. Repeat steps 4 through 7 for each layer of data. Save the composite images.

3-D RECONSTRUCTION

1. Open the Reconstruct© software.
2. Create a new series by clicking “series -> new” and importing the JPEG EDS images from each layer. If a mosaic of 2-D EDS images was used, import the JPEG images created with the composite image creation procedure. Input the pixel size in µm from the XGT-7000™ software and click “import.” Close this window.
3. Click on “section -> list sections.” Select layer 1 and click “modify -> thickness.” Input the depth polished down for layer 2. Repeat this process for each layer, using the correct respective polishing depths. Assume that the final layer has a thickness equivalent to the X-Ray penetration depth calculated in step 5 of the parallel polishing procedure.
4. Using the various tracing tools, trace a feature of interest on layer 1. Go to layer 2 and trace the next layer of the same feature traced on layer 1. Continue this for each layer. If there are multiple seemingly separate features throughout the layers, trace each individual inclusion throughout each layer in this manner, otherwise Reconstruct© might not assume them to be separate. This process is called “segmentation.” If the features are very distinct in the images, the “wildfire” region growing tool might be used successfully. However, this method is temperamental and can often result in incorrect feature segmentation.
5. In addition, it is necessary to create a 3-D “scalecube” in the reconstruction. To do so, trace a square on the first layer of data, keeping in mind that each pixel corresponds to a certain length. Trace this square identically on as many layers of data as needed to make a useful scalecube. The lengths on each side of the cube can be labeled once the reconstruction is exported as a JPEG file.

6. Click “object->list objects.” Double-click each “domain” to add it to the 3-D scene. Ideally, each “domain” will represent an individual feature, or the scalecube. If this is not the case, ensure that step 12 was carried out correctly. A 3-D scene of the selected domains will be created. In order to change how Reconstruct represents the 3-D scene, go to “series->options->3-D.”
7. Save the series and export the 3-D scene from the 3-D scene window if needed.

2.6 Acquiring Scanning Electron Microscope (SEM) Data

This section will describe how to acquire SEM data for additional characterization of the feature of interest. There are two sections for SEM characterization: acquiring secondary electron (SE) or backscatter electron (BSE) images, and acquiring SEM EDS data. If SEM data are not needed, this section may be skipped. This process could theoretically be carried out on every layer of a specimen during serial polishing. However, the specimen must remain attached to the custom polishing mount created for the XGT-7000™ custom stage; otherwise, 2-D indexing will not be easily possible. For this study, the SEM was used to obtain high-resolution and high-magnification images of the feature of interest. It was also used for the detection of light elements, as the available JEOL® JSM-5610™ is equipped with an Oxford Instruments® INCAx-act™ 51-ADD0021 light element detector that the XGT-7000™ does not have.

2.6.1 Acquiring SE or BSE Images

1. Using the serial polisher, polish the specimen down to a very smooth surface finish free of any scratches or defects. Usually, diamond polishing media are required to achieve a final surface finish of approximately 1 µm.

2. Follow the SEM manufacturer's instructions for venting the chamber and mounting the specimen inside of the SEM [21].
3. Turn on and slowly saturate the electron source filament.
4. Choose an appropriate spot size and working distance.
5. Bring the specimen into focus and locate the feature of interest.
6. Acquire SE images of the feature of interest at an appropriate magnification, according to the manufacturer's instructions [21]. Etching may be required to produce contrast in SE images of some specimens. Etching procedures are material specific.
7. If there is no contrast between the feature of interest and the bulk region of the specimen, a BSE detector may be necessary. Insert the backscatter detector and switch the SEM over BSE detector mode to check if the BSEs give better contrast for the feature of interest. Follow the manufacturer's instructions for acquiring BSE images [21].

2.6.2 Acquiring SEM EDS Data

This process is only necessary if higher spatial-resolution EDS maps are desired, or if the available SEM has a light element detector that could be useful for characterization purposes.

1. Start the SEM EDS software.
2. Follow the manufacturer's instructions for acquiring either spot scans or 2-D EDS maps of the desired features of interest [21].
3. Export the quantification data from the spot scans or JPEG images from the 2-D EDS maps.

2.7 ACQUIRING OPTICAL MICROSCOPY IMAGES

This process is used for acquiring optical microscope images of the specimen and feature of interest. This procedure could theoretically be carried out on each layer during serial polishing, as long as the specimen remains attached to the custom polishing platen.

1. Using the serial polisher, polish the specimen down to a very smooth surface finish free of any scratches or defects. Usually a diamond polishing media is required, as it is necessary to achieve a final surface finish of approximately 1 µm.
2. Follow the microscope manufacturer's instructions for acquiring optical microscope images at an appropriate magnification [22]. If there is no contrast between the feature of interest and the bulk material, etching may be required. Use an appropriate etchant and acquire optical images of the etched feature of interest.

Chapter 3: Technique Demonstration

3.1 TEST SPECIMENS

An Alloy 718 composition standard was acquired from Ted Pella, Inc. to test the quantification accuracy of the Horiba® XGT-7000™ and to use as a reference standard. In a separate exercise, a trial specimen was used to demonstrate that the techniques developed and described in the previous chapter are appropriate for quantifying the morphologies of element distributions, and are, thus, applicable for the study of white spots in Alloy 718. A United States post-1982 penny was used as the trial test specimen because it has a zinc interior with an approximately 15-μm thick copper cladding, features amenable to demonstrating the techniques developed. The zinc interior and copper exterior provide good contrast in XRF EDS data analysis. The surface features of the penny also provide changes in thickness that are of dimensions similar to the size of white spot features. All of the above qualities make the penny a good candidate for determining whether or not the spatial resolution and mapping capabilities of the equipment and experimental procedures will be useful for characterizing defects in Alloy 718 specimens.

3.2 PROCEDURES

The procedures for testing the XRF EDS technique are presented in two parts: standard comparison and test specimen analysis. The standard comparison section will determine the capabilities of the XRF EDS system for measuring element concentrations in an Alloy 718 standard specimen with a known composition. The test specimen analysis section will detail how

the entire serial polishing technique is tested on a specimen with features on the same length scale as anomalies in Alloy 718.

3.2.1 Standard Comparison

In order to quantify the accuracy of the XGT-7000™ for composition analysis, a standard Alloy 718 specimen was analyzed under the conditions listed in Table 3.1.

Table 3.1: XGT-7000™ Standard Specimen Analysis Operating Conditions

Voltage	50 keV
Time	900 s
Current	Auto (mA)
Process Time	6 (unitless)
X-Ray Tube Diameter	400 µm

Five separate spectra from random areas on the standard specimen were acquired and quantified under these conditions. The quantified compositions were then analyzed and compared to the reported composition of the specimen. Figure 3.1 shows an example of an acquired Alloy 718 standard XRF EDS spectrum.

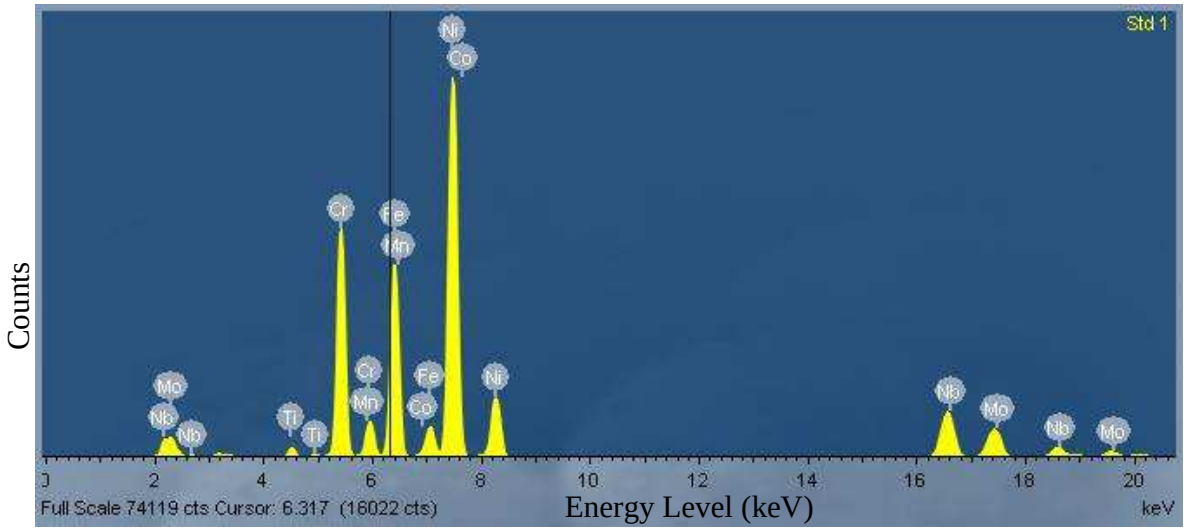

Figure 3.1: An example Alloy 718 standard specimen spectrum.

Table 3.2 shows the results of the comparison between the acquired spectra and the reported composition of the standard specimen. The “observed composition” is an average of the quantification results from the five scans. The “observed standard deviation” is the statistical standard deviation in composition measured from the quantification results of the five different scans.

Table 3.2: Elemental composition of Alloy 718 standard specimen (wt%). Observed are from XGT-7000™ analysis and Reported are data supplied by the standard specimen vendor.

Element	Reported Standard Composition [23]	Observed Composition	Absolute Difference (wt%)	% Difference	Observed Std. Deviation
Al	0.56	0.58	0.02	0.04	0.02
Si	0.14	0.09	-0.05	-0.43	0.01
Ti	1.01	1.07	0.06	0.06	0.01
Cr	18.51	18.49	-0.02	0.00	0.05
Mn	0.11	0.14	0.03	0.23	0.02
Fe	18.82	18.96	0.14	0.01	0.04
Co	0.25	0.28	0.03	0.13	0.02
Ni	52.23	52.23	0.00	0.00	0.10
Nb	5.10	5.09	-0.01	0.00	0.03
Mo	3.08	3.06	-0.02	-0.01	0.01

The differences between vendor-reported and observed compositions are less than 0.10 wt% for all elements except Fe. The Fe energy peaks overlap with Mn and Co. As a result, the accurate determination of Fe composition from the energy spectrum, see Figure 3.1, is the most difficult among the elements of Table 3.2. These results show that the XGT-7000™ is capable of elemental composition measurement accuracies of better than 0.10 wt% for all elements in Table 3.2, except for Fe, for which the accuracy is approximately 0.14 wt%.

3.2.2 Test Specimen Analysis

The procedures for analyzing the penny test specimen are presented in three parts: Specimen preparation, data acquisition, and data analysis.

SPECIMEN PREPARATION

In order to test the serial polishing techniques provided in the previous chapter, the profile of a penny was observed. The following steps were followed to obtain data from the penny:

1. Section the penny in half, lengthwise, i.e., leave semicircular shapes.
2. Encapsulate the penny in phenolic resin, with its long axis horizontal and sectioned surface exposed. See Figure 3.2.

Figure 3.2: A penny encapsulated in phenolic resin.

3. Mount the specimen on the custom polishing mount.
4. Calibrate the serial polisher and polish for three minutes with the following settings: 200 rpm, 200 gram polishing load, 2400 grit silicon carbide paper. This will provide parallelism for the first layer.

DATA ACQUISITION

Two types of data were acquired from the penny test specimen. The first data acquired were spot scans from the Cu and Zn regions of the penny. The second data were 2-D XRF EDS maps of the profile, which were used to create a small reconstruction of a section of the penny.

SPOT SCANS

Spot scans were acquired in order to test the difference between the quantification accuracy of the 400 µm and 10 µm X-ray spot sizes. A 400 µm and a 10 µm spot scan were acquired in both the Cu and Zn regions with the settings listed in Table 3.3.

Table 3.3: Penny Spot Scan Operating Conditions	
Voltage	50 keV
Time	900 s
Current	Auto (mA)
Process Time	6 (unitless)

2-D XRF EDS MAPS

The experimental procedures discussed in Chapter 2 were followed for each layer of data acquired from the penny specimen. The XRF EDS mapping equipment was set up as shown in Table 3.4.

Table 3.4: Penny XRF EDS Map Operating Conditions	
Voltage	50 keV
Current	1 mA
Process Time	5 (unitless)
X-Ray Tube Diameter	10 µm
Survey Time per Frame	100 s
Pixel Width	10 µm
Accumulations	2 times
Resolution	256 pixels

Six layers of data were acquired. Based on an X-ray penetration depth of 25.0 µm in zinc and 22.0 µm in copper, it was desired to remove at least 30 µm of material between each layer of data. These values of X-ray penetration depth were calculated using equation (2) in Chapter 2. A value of 0.95 for I/I_o was used. Values of µ used for Cu and Zn were 2.613 cm^2/g and 2.892 cm^2/g, respectively [20]. The densities used for Cu and Zn were 8.92 g/cm^3 and 7.14 g/cm^3, respectively [24]. The specimen was polished for 45 seconds with 2400 grit abrasive paper between each layer in order to achieve a polishing depth of approximately 80 µm between layers. The rest of the polisher settings were the same as in step 4 of the specimen preparation procedure of section 3.2.2.

DATA ANALYSIS

The spot scans from the different sections of the penny were quantified using the XGT-7000™ software. The data analysis procedure from Chapter 2 was followed exactly to create the 3-D reconstructions of the penny.

TEST SPECIMEN ANALYSIS RESULTS

Table 3.5 shows results from the XRF EDS spot scans in the Cu and Zn regions of the penny. One spot scan with each size capillary was taken for each region of the penny. The compositions aquired with the different capillary sizes are compared to each other for the Zn and Cu regions, separately.

Table 3.5: Penny XRF EDS Spot Scan Analysis

	Area of Penny							
	Zn				Cu			
	Composition (wt %)				Composition (wt %)			
	Capillary Size		Absolute Difference (wt%)	% Diff.	Capillary Size		Absolute Difference (wt%)	% Diff.
Element	400 µm	10 µm			400 µm	10 µm		
Al	0.55	0.69	-0.14	-0.25	0.30	0.39	-0.09	-0.30
Si	0.57	0.25	0.32	0.56	0.27	0.13	0.14	0.52
Fe	0.02	0.02	0.00	0.00	0.04	0.03	0.01	0.25
Cu	0.73	0.71	0.02	0.03	74.41	73.81	0.60	0.01
Zn	98.13	98.33	-0.20	0.00	24.98	25.64	-0.66	-0.03

The large amount of Zn present in the Cu region scans is most likely due to the X-rays penetrating deeper than the thickness of the Cu cladding on the exterior of the penny. It could also be a result of the use of a copper alloy, such as brass, for the cladding. These results show that there is no greater than a 0.66 wt% variation for any element between the compositional

quantifications using the 400 µm and 10 µm spot sizes, and the percentage difference for Cu and Zn are less than 0.05%. Al and Si vary by a percentage difference of up to 0.56%, but there are very low levels of these elements, and quantification is less accurate at count numbers around 55. The 400 µm spot size is assumed to be more accurate than the 10 µm spot size due to increased signal, so it will be used for quantifying composition in this study. However, the 10 µm spot size is still accurate to within 1.0 wt% or less, with a much higher spatial resolution than the 400 µm spot size, so it was used to create 2-D EDS maps.

The yellow box in Figure 3.3 shows the region of the penny that was examined using serial polishing techniques and XRF EDS analysis.

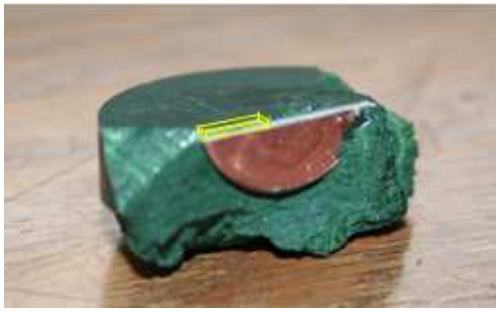

Figure 3.3: The sectioned penny is shown broken out of its phenolic encapsulation. The region examined is highlighted by the yellow box.

Figures 3.3 and 3.4 provide example 2-D composite XRF EDS area maps stitched together from multiple scan areas. Images like these were used to produce 3-D reconstructions of the internal composition of the penny.

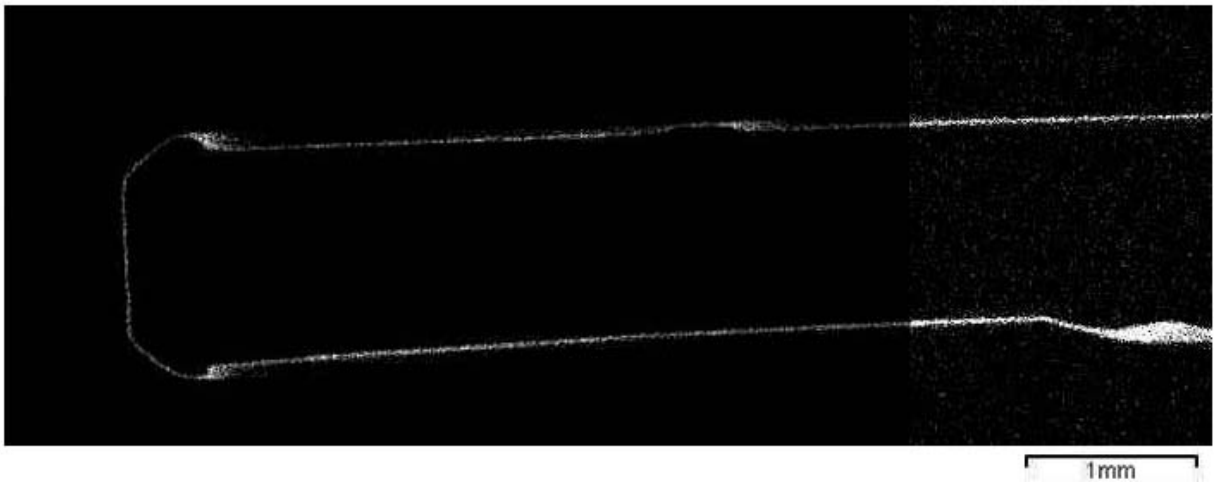

Figure 3.4: Cu EDS map of one layer of the penny.

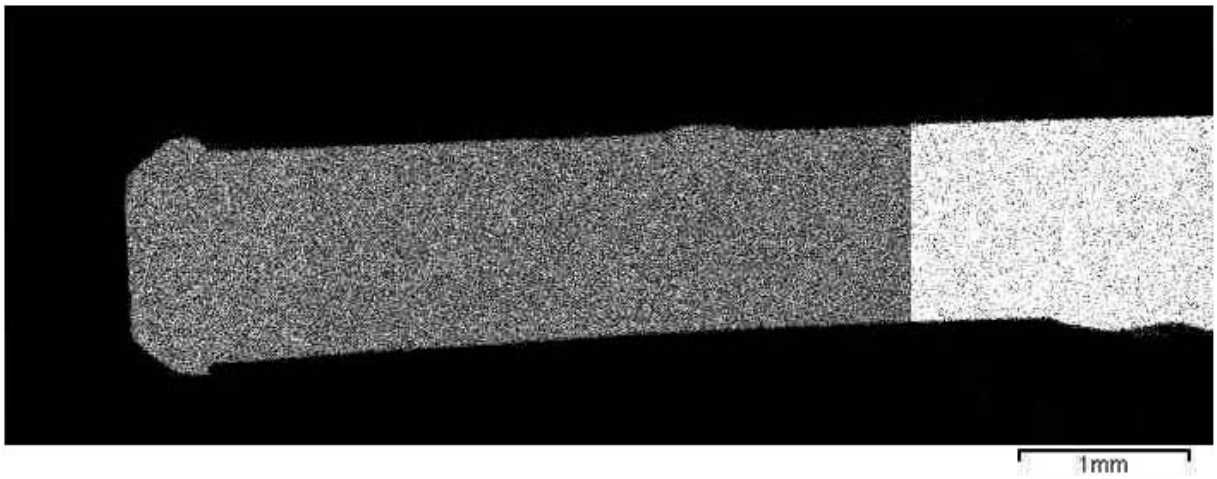

Figure 3.5: Zn EDS map of one layer of the penny.

The cause of variation in intensity between the multiple images used to create the mosaic above is normalizing errors. However, the variation in intensity does not affect the ability to create 3-D reconstructions from the 2-D images.

Figure 3.6 shows an example image of a layer that has been segmented by hand in Reconstruct®. The image that is segmented is one layer of the Cu EDS data. This segmentation process was carried out for each layer of data, for both the Cu and Zn maps. The segmented layers are used by Reconstruct® to create 3-D representations of the data.

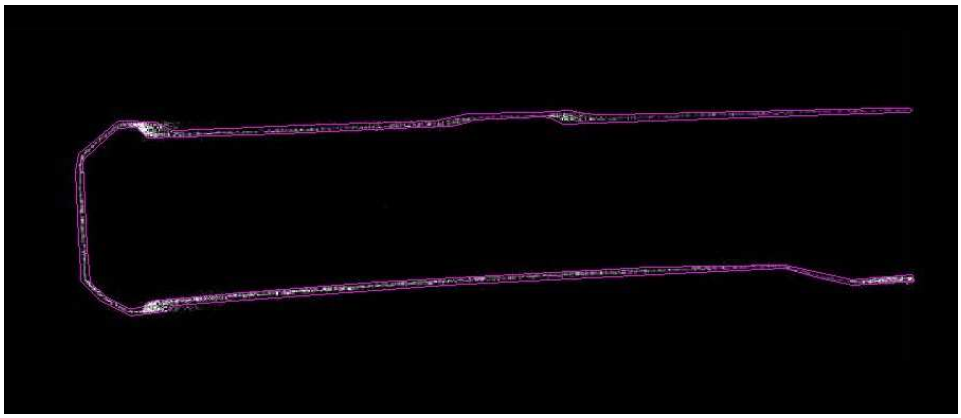

Figure 3.6: A segmented layer of Cu EDS data.

Figure 3.7 is a 3-D reconstruction of the section of the penny that was created using XRF EDS maps for copper. It shows the copper cladding around the penny. Changes in overall thickness of the penny are shown, and these reveal the surface features of the coin. Figure 3.8 was created using XRF EDS maps for zinc and shows the interior the penny. Figure 3.9 is a top view of the copper cladding, showing changes in thickness due to surface features.

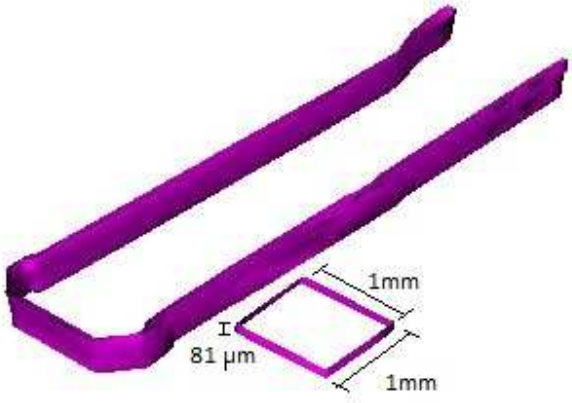

Figure 3.6: A 3-D reconstruction of the copper cladding of the penny.

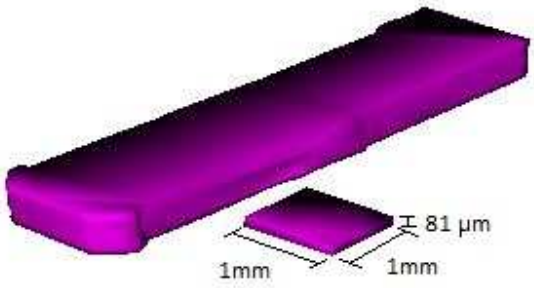

Figure 3.7: A 3-D reconstruction of the zinc interior of the penny.

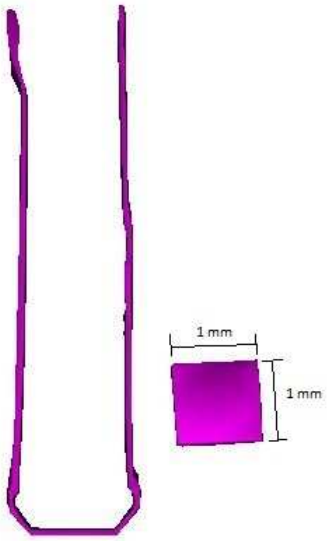

Figure 3.8: A 3-D reconstruction of the copper cladding of the penny, top view.

In order to determine the spatial accuracy of the reconstruction technique, the thickness of the penny was measured five times with three different methods: by using vernier calipers; by measuring thickness on the 2-D EDS maps; and by measuring segmented layers in Reconstruct®. There are some significant variations in the measured thickness of the penny, depending on which method is used. Errors for the original measurements are represented by the standard deviations of the measurements. These errors present themselves as human-introduced measurement errors, related to not measuring exactly perpendicular to the penny faces. For the calipers, EDS Maps, and Reconstructions, these measurement errors are 0.020 mm, 0.005 mm, and 0.008 mm, respectively. In addition, the EDS maps have experimental errors equal to the X-ray interaction width, due to the X-ray spot being only slightly on the material, thus sending out

less signal and not properly representing the exact location of the edge. It is assumed that the X-ray interaction volume is a half-sphere with a radius equal to the X-ray penetration depth [25]. Thus, an X-ray interaction width of 44.0 µm, equal to twice the X-ray penetration depth in Cu, was used.

The reconstruction has an additional source of human-introduced error, related to the free-hand segmentation technique. This error was measured to be 0.006 mm. The various sources of error for each measurement method were combined using a root-sum-squares (RSS) method [29]. A summary of the thicknesses and errors can be seen in Table 3.6. Error values for the "differences" column in Table 3.6 were calculated by combining the errors for the two measurement techniques involved using a root-sum-square method.

Table 3.6: Penny Spatial Accuracy Analysis

	Average Measured Thickness (mm)		Differences (mm)
Calipers	1.264 ± 0.019	EDS vs. Calipers	0.037 ± 0.036
EDS Maps	1.301 ± 0.031	Reconstruction vs. Calipers	0.046 ± 0.022
Reconstruction	1.310 ± 0.010	Reconstruction vs. EDS	0.009 ± 0.033

These elemental quantifications and images show that the XRF/EDS technique can achieve spatial accuracy in 2-D maps of approximately 31 µm. When using the 400µm capillary and settings listed in Table 3.3, the compositional quantification capability of the XRF EDS system has an accuracy of better than 0.10 wt% for all elements except Fe, for which an accuracy of 0.14 wt% is possible. The two different X-ray capillary sizes provide elemental quantifications with less than 1.0 wt% difference for elements that are present in large quantities, and less than 0.5 wt% difference for trace elements. The two different capillary sizes provide

elemental quantifications with less than 0.05 % difference for elements present in large quantities. The error in spatial measurements for the final 3-D reconstruction is approximately 55 µm. This number is a RSS combination of independent measurement errors for both the 2-D EDS maps (31 µm), reconstruction process (10 µm), and experimental error of the EDS technique related to X-ray interaction width (44 µm). For this study, the same technique will be applied to features in Alloy 718.

Chapter 4: Data Set Production

4.1 INTRODUCTION

The purpose of this chapter is to describe the specimen and experimental parameters used to produce Alloy 718 data sets. Great care must be taken while preparing specimens to ensure proper 3-D indexing and accurate compositional analysis for each layer of data. XRF EDS data must be acquired using appropriate settings for the Horiba XGT-7000^{TM} instrument. Post-processing software must then be used in a way that clearly and accurately displays the desired information.

4.2 SPECIMEN DESCRIPTION

The specimen observed in this study is a piece of Alloy 718, acquired from an Alloy 718 billet that had been rolled down from a VAR ingot. A slice of the billet containing a dirty white spot was acquired from a commercial supplier that is a member of the Special Metals Processing Consortium. The observed specimen was sectioned from the billet slice using wire electrical discharge machining (EDM) methods. The final, sectioned specimen of interest is a 1”x1”x1” cube of Alloy 718, with the dirty white spot present in the center of one face of the cube. Figure 4.1 is an image of the original billet slice provided by the commercial supplier, the sectioned specimen of interest, and a small piece of scrap material.

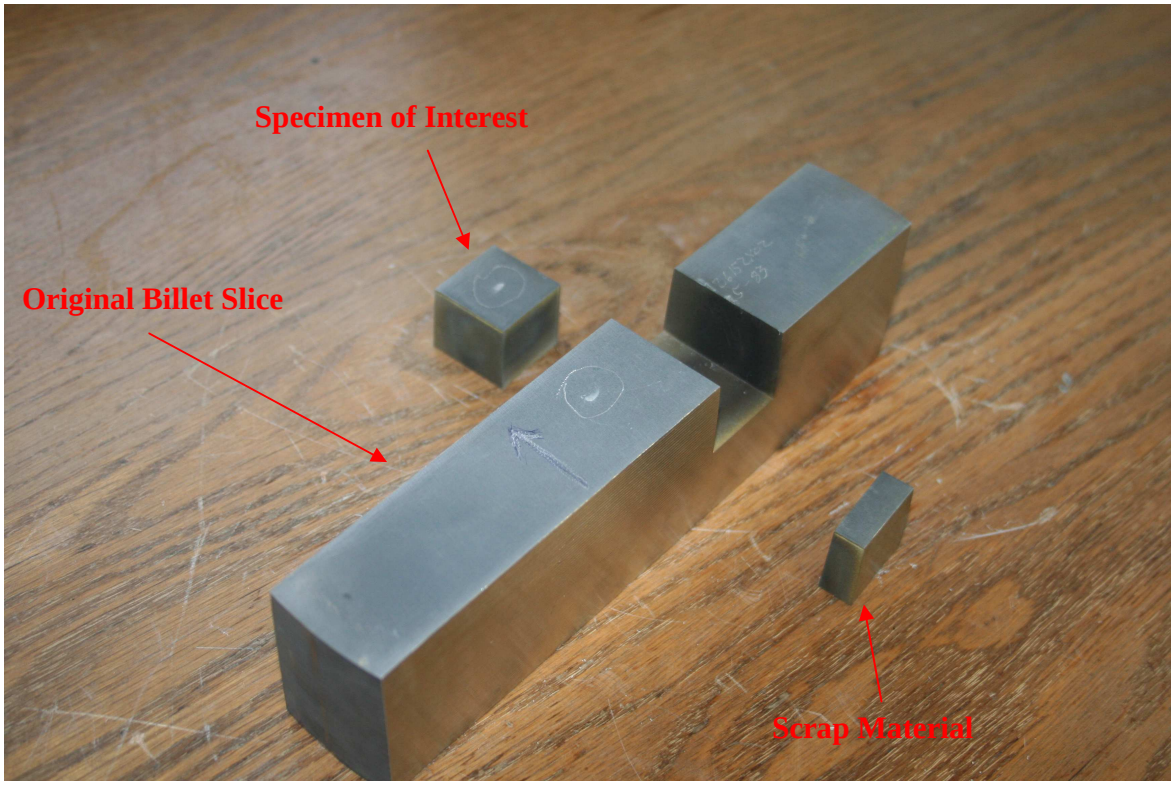

Figure 4.1: The original billet slice, which has had a specimen containing a dirty white spot sectioned out.

Figure 4.2 shows a schematic representation of the billet slice, relative to the entire billet disc that the slice was obtained from. The directions c, r, and h represent the circumferential, radial, and height directions of a cylindrical coordinate system used to discuss compositional trends later in this paper. The dirty white spot of interest is represented by the grey area, with the darker grey region being the Ti-rich side of the white spot.

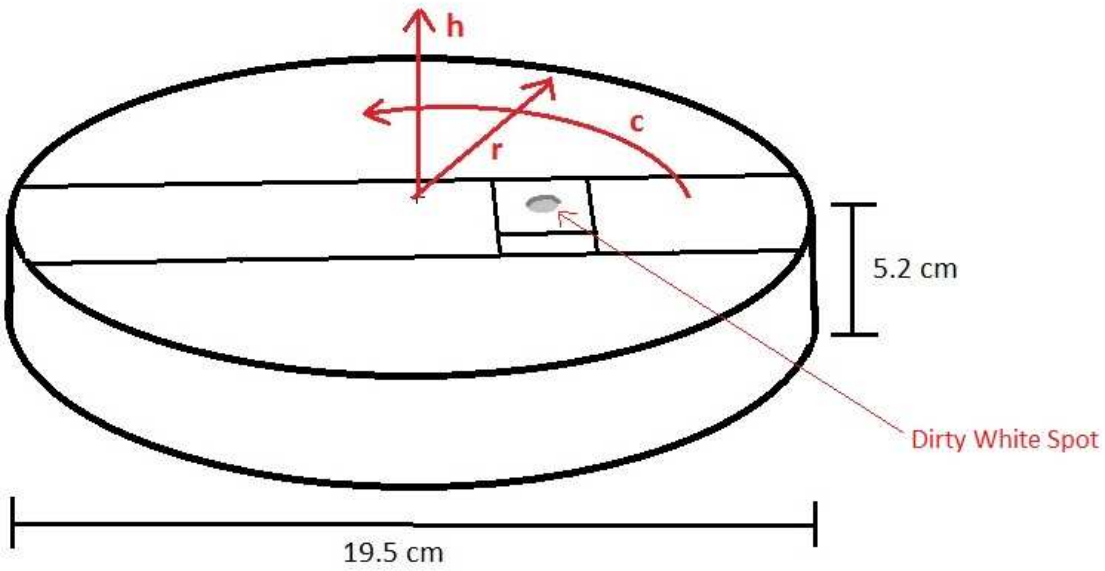

Figure 4.2: Schematic representation of the sectioned billet slice (note: image is not to scale).

Figure 4.3 shows an optical image of the dirty white spot, acquired at 5x magnification. The dirty white spot was lightly etched (Kalling's No. 1 etchant, as described in Section 4.3.3) in this image. This dirty white spot is the feature of interest to be observed with XRF EDS, SEM, and optical microscopy techniques.

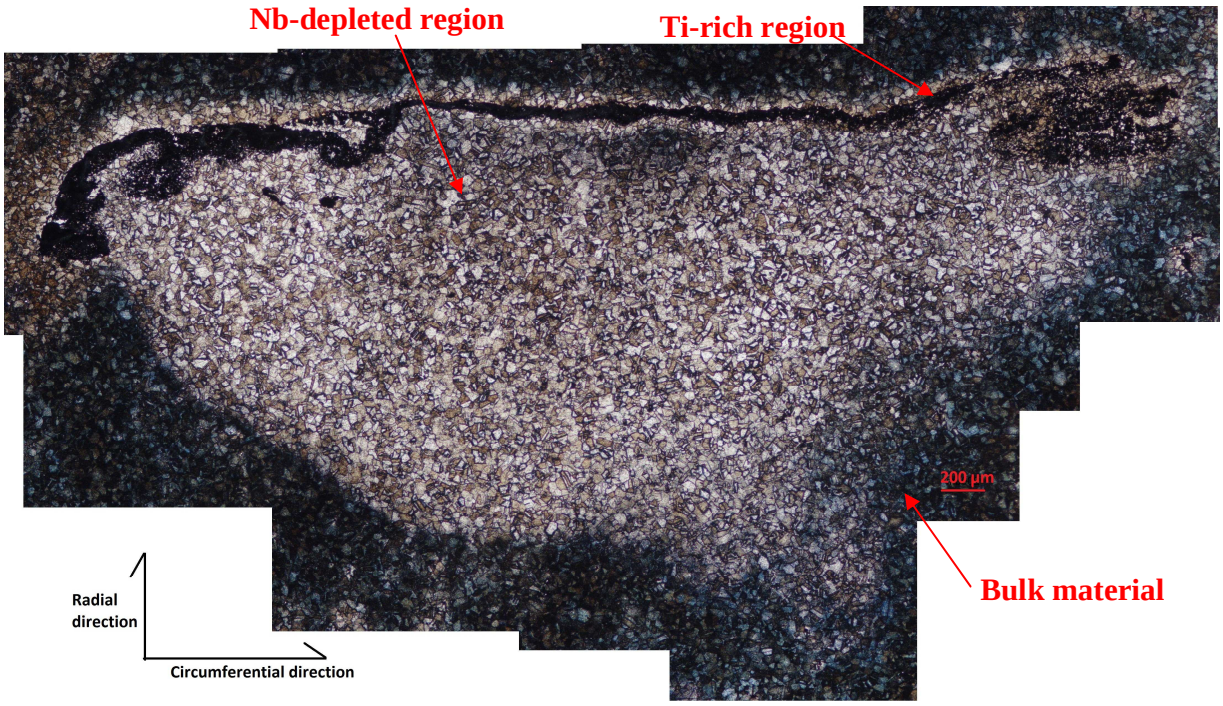

Figure 4.3: An image of the dirty white spot contained in the specimen of interest, etched.

4.3 HARDWARE SETUP

This section describes proper use of the serial polisher, XRF EDS system, SEM, and optical microscopy equipment.

4.3.1 Serial Polisher

Parallelism between the sequentially-polished specimen layers must be provided by the serial polisher to enable proper indexing of 3-D data sets. Follow the calibration procedure in the Allied High Tech, Inc. Multiprep™ user's manual. This procedure should produce platen-specimen holder parallelism of at least ± 1 µm across a 57.15 mm width (1.75×10^{-5} rad) [17]. The final parallelism of the specimen surface will not be as precise as this value. Final specimen

surface parallelism of ± 10 µm/25.48 mm (3.92×10^{-4} rad) or better, as shown in Table 2.2, was achieved. This calibration procedure must be repeated between each serial polishing section (approximately 60 µm of depth removed), as the serial polisher head can shift during normal use. At the beginning of the serial sectioning process, it is generally a good idea to double-check parallelism of the polisher with a piece of scrap material before polishing the specimen of interest.

While the polishing precision discussed above places a practical lower bound on the depth of layers, there is also a layer depth requirement based on the penetration depth of X-rays into the alloy. Using Equations (2.1) and (2.2) from Chapter 2, an X-ray penetration depth of approximately 31 µm at an accelerating voltage of 50 keV was calculated for Alloy 718. See Table 2.3 for the values used in these calculations. A polishing depth of approximately 60 µm was chosen for the Alloy 718 specimen to ensure no overlap in the XRF EDS results between layers. A lower accelerating voltage could be used to acquire thinner layers, but this would negatively affect signal levels and quantification results. For the XGT-7000™, a surface finish produced by 600 grit Si-C paper is adequate to eliminate any effect of surface roughness on the XRF EDS data. In order to achieve this polishing depth and surface finish for analysis in the XGT-7000™, the following polishing procedure was followed. Ultrasonic cleaning using a basic degreaser and rinsing with deionized water was applied between all polishing steps. A 5 gram load was used for a relatively large surface area being polished, 1.0” x 1.0”.

1. Polish for 5 min. with 120 grit Si-C paper at 300 rpm and a 5 gram load.
2. Polish for 5 min. with 240 grit Si-C paper at 300 rpm and a 5 gram load.
3. Polish for 5 min. with 400 grit Si-C paper at 300 rpm and a 5 gram load.
4. Polish for 5 min. with 600 grit Si-C paper at 300 rpm and a 5 gram load.

For the SEM and optical microscope, a surface finish provided by a 1 µm diamond polishing medium is desired, as secondary-electron (SE) and back-scattered-electron (BSE) images are needed, in addition to SEM EDS data. In order to achieve this surface finish, the following polishing procedure was followed, with ultrasonic cleaning using a basic degreaser and subsequent rinsing with deionized water between all polishing steps. A reduced 3 gram load was used for this procedure.

1. Polish for 10 min. with 240 grit Si-C paper at 200 rpm and a 3 gram load.
2. Polish for 10 min. with 320 grit Si-C paper at 200 rpm and a 3 gram load.
3. Polish for 10 min. with 400 grit Si-C paper at 200 rpm and a 3 gram load.
4. Polish for 10 min. with 500 grit Si-C paper at 200 rpm and a 3 gram load.
5. Polish for 10 min. with 600 grit Si-C paper at 200 rpm and a 3 gram load.
6. Polish for 10 min. with 1200 grit Si-C paper at 200 rpm and a 3 gram load.
7. Polish for 10 min. with 2400 grit Si-C paper at 200 rpm and a 3 gram load.
8. Polish for 10 min. with 4000 grit Si-C paper at 200 rpm and a 3 gram load.
9. Polish for 5 min. with 15 µm diamond polishing media and polishing cloth at 200 rpm and a 3 gram load.
10. Polish for 5 min. with 9 µm diamond polishing media and polishing cloth at 200 rpm and a 3 gram load.
11. Polish for 5 min. with 3 µm diamond polishing media and polishing cloth at 200 rpm and a 3 gram load.

12. Polish for 5 min. with 1 µm diamond polishing media and polishing cloth at 200 rpm and a 3 gram load.

For both polishing procedures listed above, the serial polisher head was set to oscillate across the polishing surface and fully rotate.

4.3.2 Horiba® XGT-7000™ Setup

Three different experimental conditions, i.e., software settings for instrument operation, were used to acquire XRF EDS data, two for spot scans and another for 2-D EDS mapping. For the 400 µm spot scans of the white spot on each layer, the hardware settings in Table 4.1 were used.

Table 4.1: 400 µm XRF EDS Spot Scan Operating Conditions

Vacuum	10^{-2} Torr
Accelerating Voltage	50 keV
Scan Time	900 s
Current	Auto
Process Time	6 (unitless)
X-Ray Capillary	400 µm

In order to acquire 10 µm spot scans, used to observe composition trends across the polished surface, the settings in Table 4.2 were used.

Table 4.2: 10 µm XRF EDS Spot Scan Operating Conditions	
Vacuum	10^{-2} Torr
Accelerating Voltage	50 keV
Scan Time	1800 s
Current	Auto
Process Time	6 (unitless)
X-Ray Capillary	10 µm

2-D EDS maps of each layer using the 10 µm X-Ray capillary were acquired using the XGT-7000™ equipment settings listed in Table 4.3.

Table 4.3: XRF 2-D EDS map settings	
Vacuum	10^{-2} Torr
Accelerating Voltage	50 keV
Current	1 mA
Process Time	5 (unitless)
X-Ray Capillary	10 µm
Survey Time per Frame	100 s
Pixel Width	0.010 mm
Accumulations	6 times
Resolution	256 pixels

In order to automatically map large areas of a specimen surface, the *multimap* software feature was used. The multimap feature of the XRF EDS software creates a mosaic of multiple EDS maps at a higher spatial resolution than would be possible with a single EDS map. It works by simply setting up the dimensions and pixel size of the first EDS map in a grid of maps and then specifying the number of maps in the grid, along both the x- and y-directions. The resulting mosaic of individual maps is then automatically created and indexed for automated data acquisition. See Table 4.4 for the settings used to create a multimap grid. These multimap settings were used with the 2-D EDS map settings provided in Table 4.3.

Table 4.4: XGT-7000™ Multimap Grid Settings	
Size X	2.56 mm
Size Y	2.56 mm
Position Left	1.2 mm
Position Right	6.4 mm
Mosaic Size X	5
Mosaic Size Y	5

4.3.3 SEM and Optical Microscope Setup

XRF EDS scans showed two distinct regions in the dirty white spot: a Ti-enriched region and a Nb-depleted region. The SEM was used to acquire BSE images of the Ti-rich region and additional EDS data of the Ti-rich region. Neither the BSE nor the SE detectors provided sufficient contrast to view the Nb-depleted region without etching. In order to acquire the BSE

images of the Ti-rich region, the SEM was adjusted to a working distance of 13 mm, a spot size of 40, and an accelerating voltage of 20 keV.

In addition to XRF EDS data, SEM EDS data were acquired to take advantage of the smaller spot sizes and higher spatial resolution possible with the SEM. With the SEM the composition of <1.0 µm scale microstructures of the Ti-rich region can be mapped. In addition, the available SEM has a light element detector, which is useful for determining the presence of oxygen and nitrogen. See Table 4.5 for the SEM operating conditions used to acquire EDS data of the Ti-rich region.

Table 4.5: SEM EDS Operating Conditions	
Working Distance	20 mm
Spot Size	43 (unitless)
Accelerating Voltage	20 keV
Process Time	6 (unitless)
Livetime	60 s
Range	20 keV
Channels	1000

Optical microscope images of the unetched Ti-rich region and etched Nb-depleted region were acquired (without polarizing filters) using a Nikon Epiphot 200 inverted microscope. In order to acquire the optical images of the Nb-depleted region, the specimen was etched using a Kalling's No. 1 etchant with a composition of 5 g $CuCl_2$, 100 mL HCl, and 100 mL Ethanol [25]. The specimen was swabbed with this etch for a few minutes while a heat gun was used to heat the surface. This process provided an adequate etch for viewing the Nb-depleted region of the

Alloy 718 dirty white spot. The optical microscope was used in accordance with the manufacturer's instructions [22].

4.4 SOFTWARE SETUP

Four software programs were used for analyzing the data acquired in this study. The XGT-7000™ comes equipped with Oxford® Inca™ EDAX software for analyzing and quantifying EDS data. Adobe® Photoshop™ Elements was used for stitching multiple EDS images together to form a single mosaic of each layer. Reconstruct© was used to convert the stacked mosaic images into 3-D representations of the features of interest [15].

4.4.1 Oxford® Inca™ EDAX Setup

To accurately quantify the spectra obtained with the spot scans, the data acquired from the Ted Pella Alloy 718 standard specimen was used as a benchmark. The Oxford® software compares this standard file to the compositions reported by Ted Pella, and adjusts the quantification algorithms based on any observed differences. These updated algorithms are then used for performing quantification analysis on the non-standard Alloy 718 spectra. The process detailed in Section 2.3.4 was followed to set this standard.

Elements must be chosen within the Oxford® software for the purposes of quantification. Because the "auto ID" function in the software can mislabel peaks, manual peak identification was performed. For spot scan data analysis, the following elements were chosen for quantification: Al, Si, Ti, Cr, Mn, Fe, Co, Ni, Nb, and Mo. These elements occur most frequently in Alloy 718. Trace amounts of S, Cu, W, V, B, C, P, Mg, Zr, Ta, and Sn may also be present in Alloy 718, but these were not considered for composition quantification [23]. These elements

were not included because the concentrations are very small, likely below the detection limits of the XRF EDS system used in this study. Quantification of such trace elements typically has a large amount of uncertainty. From the spot scan data, relative wt% differences in Ti and Nb from the bulk material were calculated for the Ti-rich and Nb-depleted areas. The composition differences for these elements were greater than for any of the other elements observed. Based on these results, it was decided to focus on the elements Ti and Nb when creating 2-D EDS maps of each layer.

4.4.2 Adobe® Photoshop™ Elements Setup

The Photomerge™ feature in Adobe® Photoshop™ Elements was used to stitch the multiple 2-D EDS maps collected at each layer into one coherent mosaic image. However, the automatic stitching function did not work well. Thus, manual stitching was necessary. The multiple 2-D JPEG images exported from the Oxford® software were merged by simply placing the images exactly next to each other as they appear in the grid set up in Section 4.2.2. Because of the high accuracy of the 2-D stage position, overlapping of the images was not necessary. Once the images were merged together, a scale bar was placed on the merged 2-D image, and the whole image was exported as a JPEG file.

4.4.3 Reconstruct© Setup

The merged JPEG images created in Photoshop™ were imported into the Reconstruct© software package to trace out the Nb-depleted and Ti-rich boundaries. This is the segmentation process for data analysis. Reconstruct© is a software that creates 3-D representations out of multiple segmented layers of 2-D data. It was originally developed for the medical field for use

with optical or SEM images [15]. The XRF EDS data images were sorted numerically from top to bottom using file names that indicate layer numbers. The pixel size was set to 10 µm, which is the pixel width used for mapping in the XRF software, see Table 4.3. The layer thicknesses in Table 4.6, measured from the subsequent polish depth below each surface from which data were acquired, were input into Reconstruct© for each corresponding layer of data.

Table 4.6: Alloy 718 Layer Thicknesses	
Layer #	Thickness (µm)
1	49.8
2	67.4
3	56.2
4	50.8
5	61.8
6	61.4
7	62.2
8	50.0
9	70.8
10	49.4
11	63.0
12	56.4
13	56.0
14	30.6*

*A value of 30.6 µm, equal to the X-Ray penetration depth in Alloy 718, was chosen for layer 14. This is because the last layer of data is assumed to represent the depth that the data came from in the specimen. Since there was no subsequent polishing following data acquisition from the last specimen layer, layer 14, there was no value of polishing depth to use for layer thickness.

The automatic tracing function in Reconstruct© did not work effectively on the images produced using the XRF EDS technique. Thus, manual tracing to segment features of interest was performed using the "freehand tracing tool". Figure 4.3 shows a comparison between

automatic and manual segmentation techniques. Upon importing the Nb-depleted region images into Reconstruct©, it was realized that the boundary between the Nb-depleted region and bulk region of the specimen was not sufficiently distinct to use these segmentation techniques. Thus, a 3-D reconstruction of the Nb-depleted region was not possible for the XRF EDS data. The Ti-rich anomaly in the specimen was sufficiently distinct to segment.

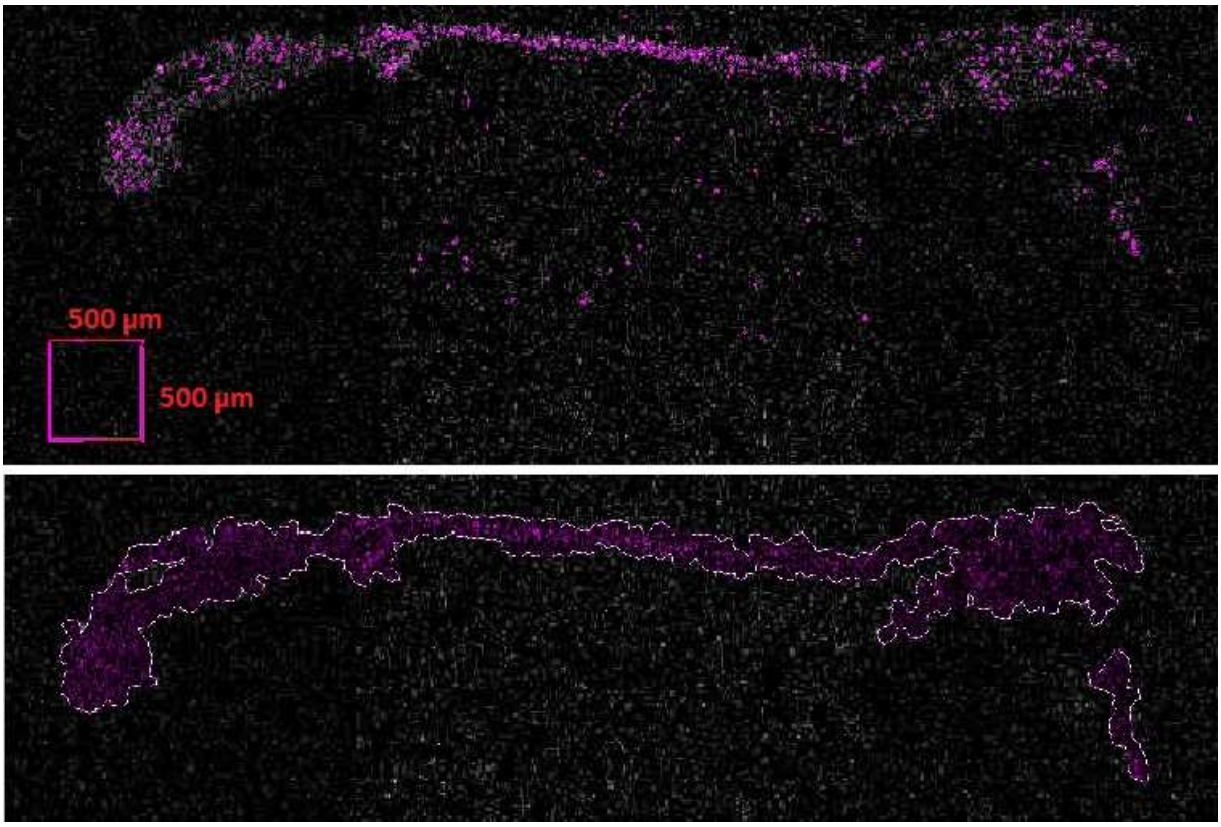

Figure 4.4: A comparison between automatic (top) and manual (bottom) segmentation techniques.

A 3-D scale feature, or "scalecube," must be created as a part of each 3-D reconstruction. This scalecube is reproduced in 3-D reconstructions to provide an appropriate length reference. In order to create the scalecube, a 2-D scale box was laid out on multiple layers of data at the

same 2-D location using the closed-point tracing tool in Reconstruct©. The box is 50 x 50 pixels, making the dimensions in 2-D 500 x 500 µm. The resulting 3-D feature is a rectangular prism with a width and length of 500 µm, and a height equal to the sum of the thicknesses of each layer it is laid out on. Figure 4.4 shows an example of a scalecube created as part of a reconstruction.

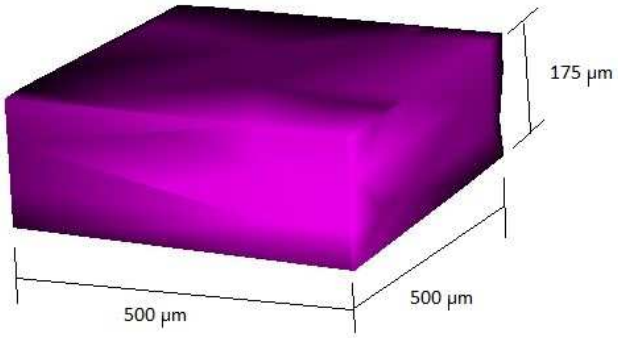

Figure 4.5: A reconstructed scalecube.

In order to view the 3-D reconstruction as a smooth, solid surface, rather than a wireframe representation, the "Boisonnat Surface" option was selected in Reconstruct©. The final 3-D reconstruction can be rotated and exported as a series of JPEG images or as a solid model. Figure 4.5 shows a comparison of the wireframe and Boisonnat surface options for representing data from the Ti-rich region.

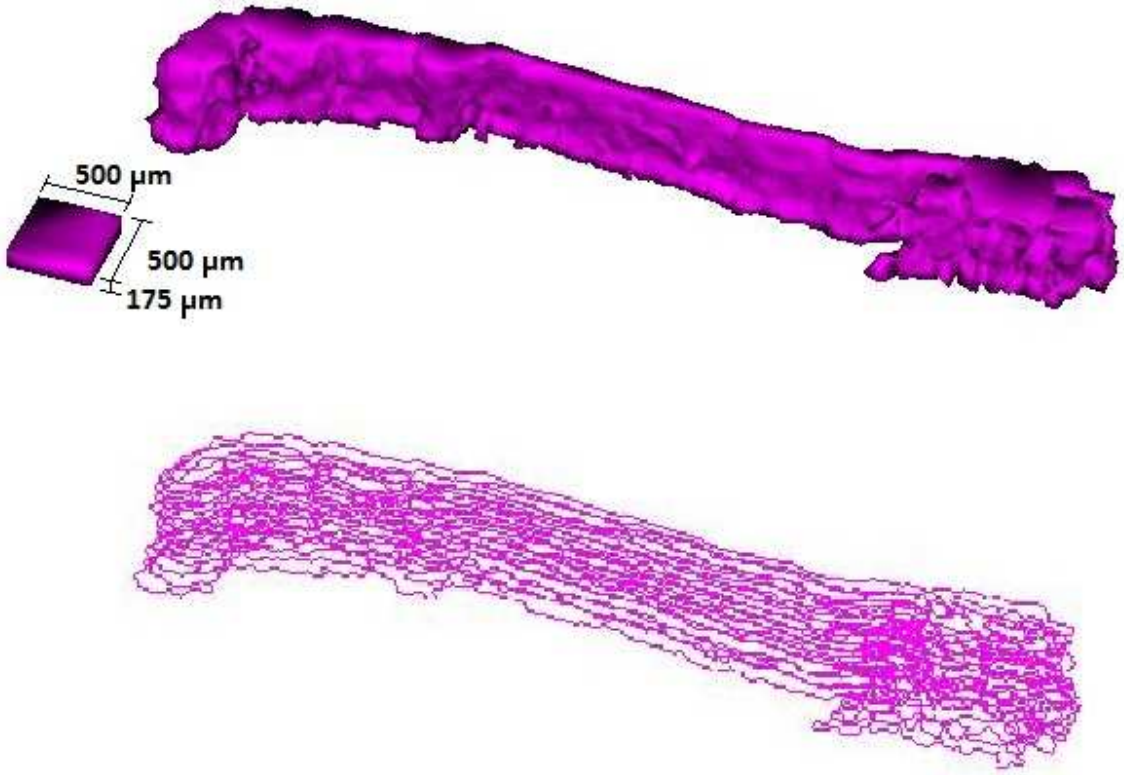

Figure 4.6: A comparison of Boisonnat (top) and wireframe (bottom) methods of representing 3-D data for the Ti-rich region.

Chapter 5: Results

5.1 INTRODUCTION

This chapter presents the results of data acquisition and analysis for the Alloy 718 specimen described in Chapter 4. This specimen was sectioned to reveal a dirty white spot that was then analyzed according to the procedure in Chapter 2 and the equipment settings detailed in Chapter 4. The goal of this analysis was to verify that the 3-D XRF EDS materials characterization technique is valid for studying anomalies in Alloy 718 ingots. It was desired to determine composition resolution capabilities of the map and spot scans to determine both feature boundary and composition detection limits. These experimental results are expected help elucidate the morphology, composition, and formation methods of the dirty white spot of interest in this Alloy 718 specimen.

5.2 2-D CHARACTERIZATION RESULTS

This section presents 2-D characterization results acquired by optical, SEM, and both XRF and SEM EDS methods. First, optical and SEM images of the selected dirty white spot are presented. Next, 2-D EDS maps from the XGT-7000™ and SEM are presented.

5.2.1 Optical and SEM Images

Optical images of the Alloy 718 dirty white spot were acquired under low magnification to give an overall picture of the anomaly being characterized by the XRF EDS technique. Figure 5.1 shows a composite optical image of the unetched Ti-rich region of the dirty white spot. The

composite image was created by taking multiple digital images covering the entire white spot area and then stitching them together in software.

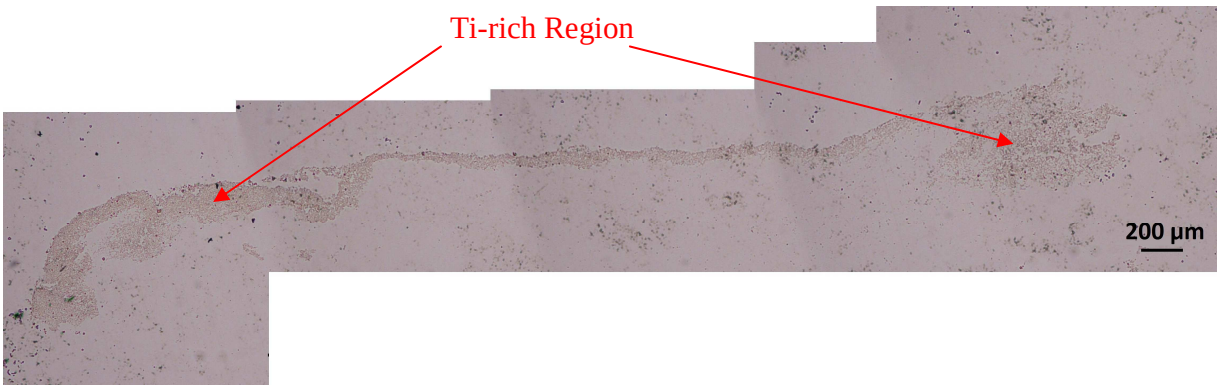

Figure 5.1: A composite image of the entire unetched Ti-rich region of the dirty white spot.

Figure 5.2 shows a composite optical image of the etched dirty white spot. The composite image was created in the same manner as Figure 5.1. The Nb-depleted region appears lighter than the bulk material and is located directly below the Ti-rich region, which is darker. Lineal intercept grain size measurements were measured from Figure 5.2 using ASTM standard E112 [30]. The average lineal intercept grain sizes of the Nb-depleted region and bulk material are approximately 24 µm and 25 µm, respectively. Measurements of each grain size were made using three random lines, with approximately 50 grain-boundary intercepts per line.

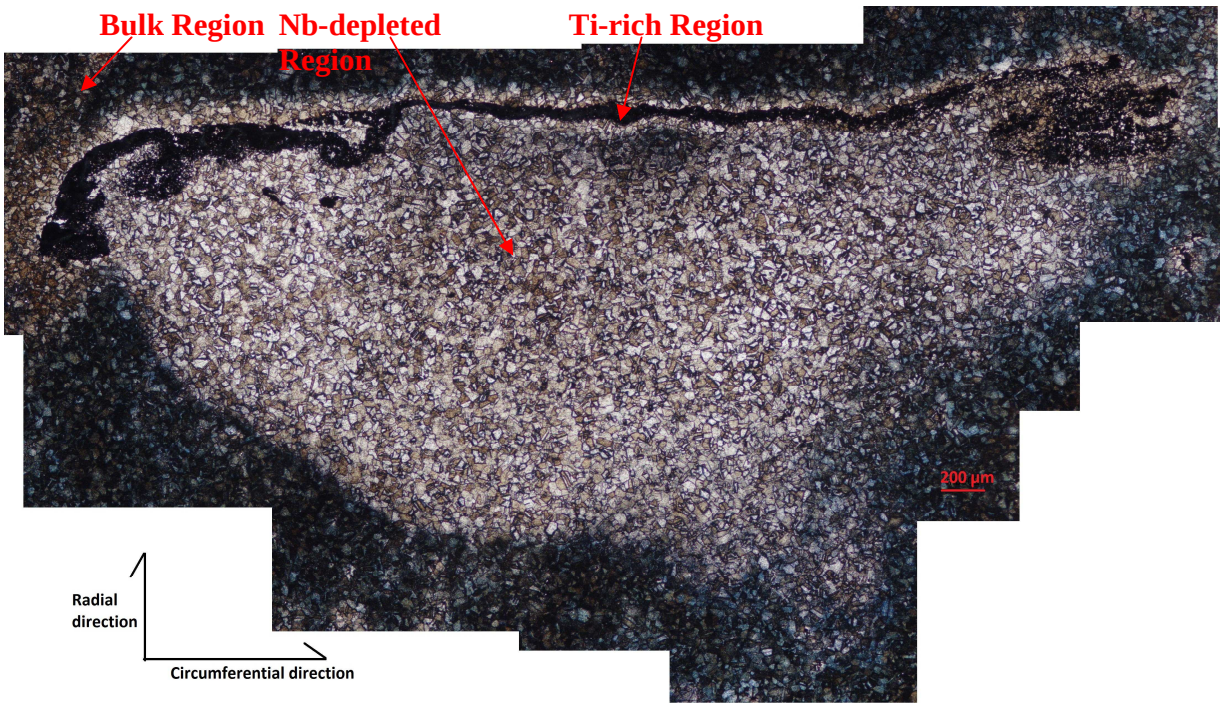

Figure 5.2: A composite image of the entire etched dirty white spot.

The SEM was used to acquire BSE images of the unetched Ti-rich region. An optical microscope was used to acquire images of the etched Nb-depleted region of the dirty white spot. The BSE detector provided insufficient contrast for viewing the Nb-depleted region without etching. This is because the BSE detector is sensitive to atomic number. In the Ti-rich region, there is a significant concentration of low-atomic number atoms, such as Ti, N or O. The average atomic number in this region is different enough from the bulk to provide contrast with the BSE detector. This is not the case for the Nb-depleted region, which is only slightly depleted in Nb. The difference in average atomic number of the Nb-depleted region relative to the bulk material is not sufficient to reveal clear contrast with the BSE detector. Due to the depletion of Nb in the white spot, etching attacked the white spot differently than the bulk material. This provided the contrast necessary to view the Nb-depleted region in the optical microscope. Figure 5.3 shows

BSE images of the unetched Ti-rich regions of the dirty white spot. Figure 5.4 shows a BSE image of the unetched Ti-rich region of the white spot at a higher magnification. The Ti-rich region contains discrete Ti-rich particles with sizes ranging from approximately 0.5 µm to 3 µm. These particles appear to be dispersed randomly in a matrix of Alloy 718 bulk material. The dark spots are most likely a compound of titanium and nitrogen (Ti-N). This identification is supported by the golden tint of the Ti-rich region in Figure 5.1, which is characteristic of titanium nitride (TiN). Quantitative analysis of the Ti-N particles is not possible with the XRF EDS system due to their being smaller than the smallest X-ray capillary available, which is 10 µm in diameter. In addition, the XRF EDS system is unable to detect N, a light element. Thus, any quantitative analysis of the Ti-rich region with the XRF EDS system will necessarily be quantifying the composition of both the Ti-N particles and their surrounding matrix.

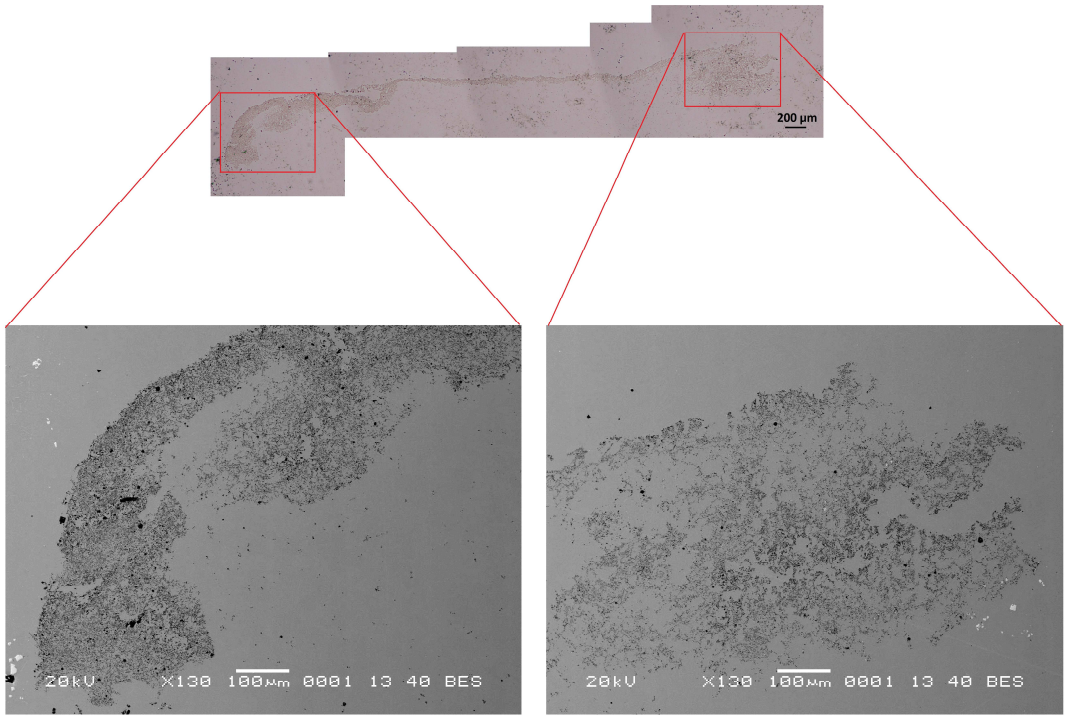

Figure 5.3: BSE images of the unetched Ti-rich region.

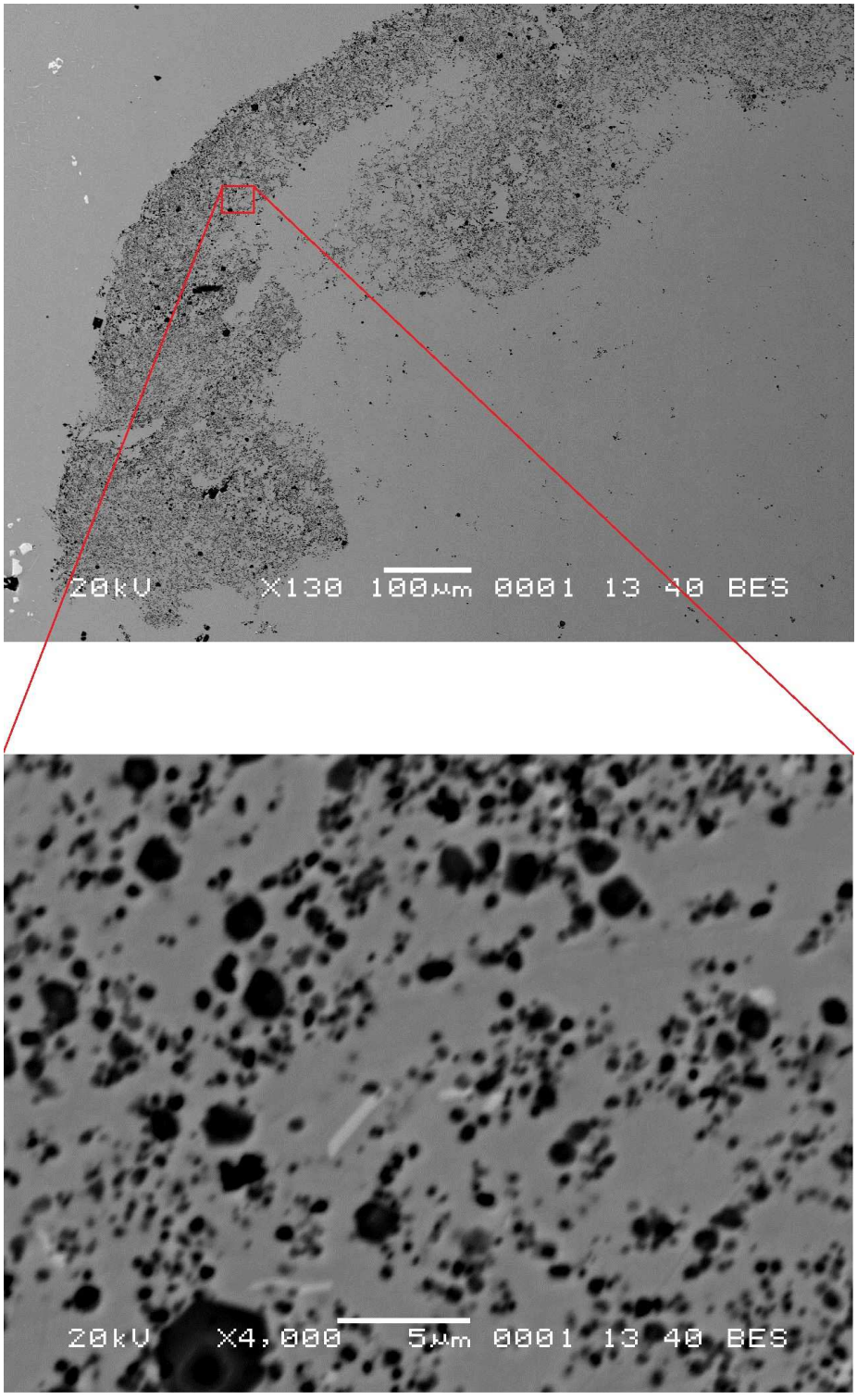

Figure 5.4: A high-magnification BSE image of the Ti-rich region.

Figure 5.5 shows a high-magnification optical image of the interface between the Nb-depleted region and the bulk material. Figure 5.6 shows a high-magnification optical image of the interface between the Ti-rich region and the Nb-depleted region. The Ti-rich region is heavily etched where the discrete Ti-N particles are present, which explains the pitted appearance.

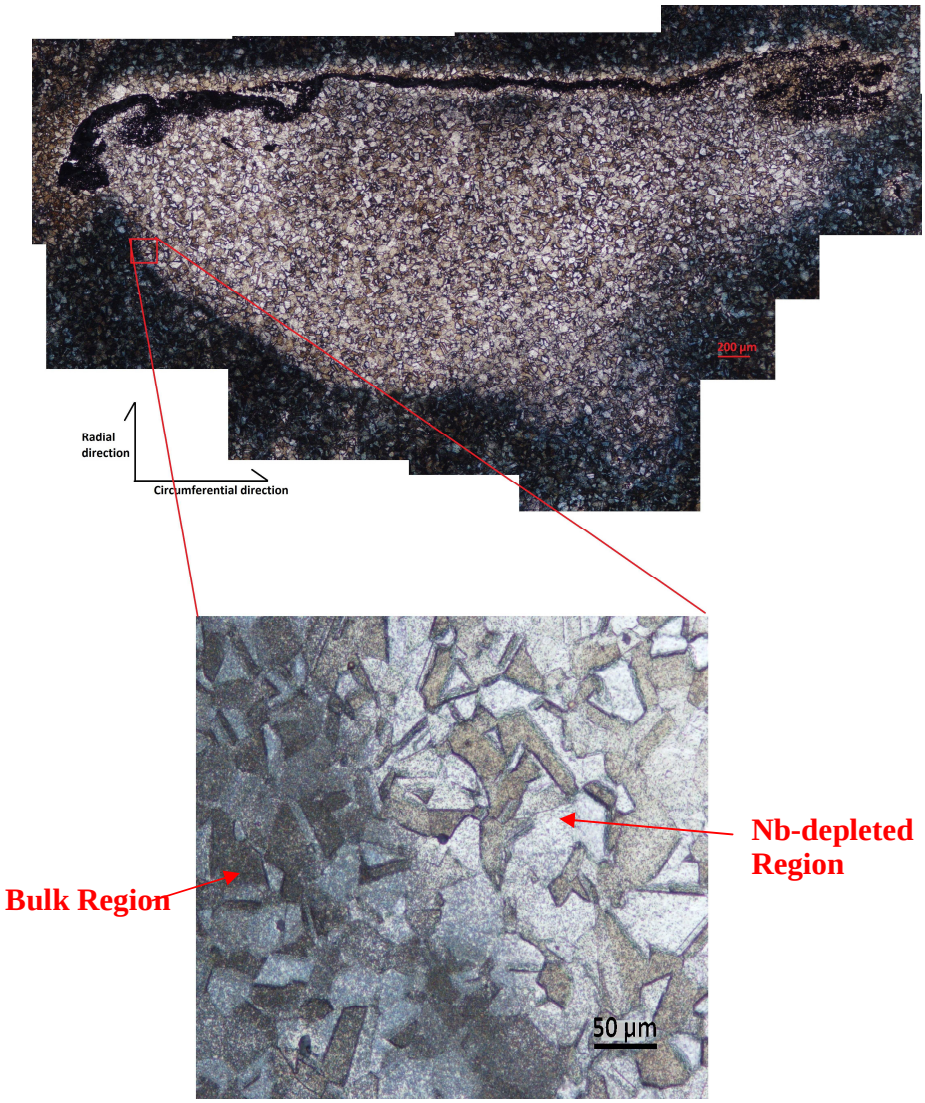

Figure 5.5: An optical image of the Nb-depleted region and bulk material interface.

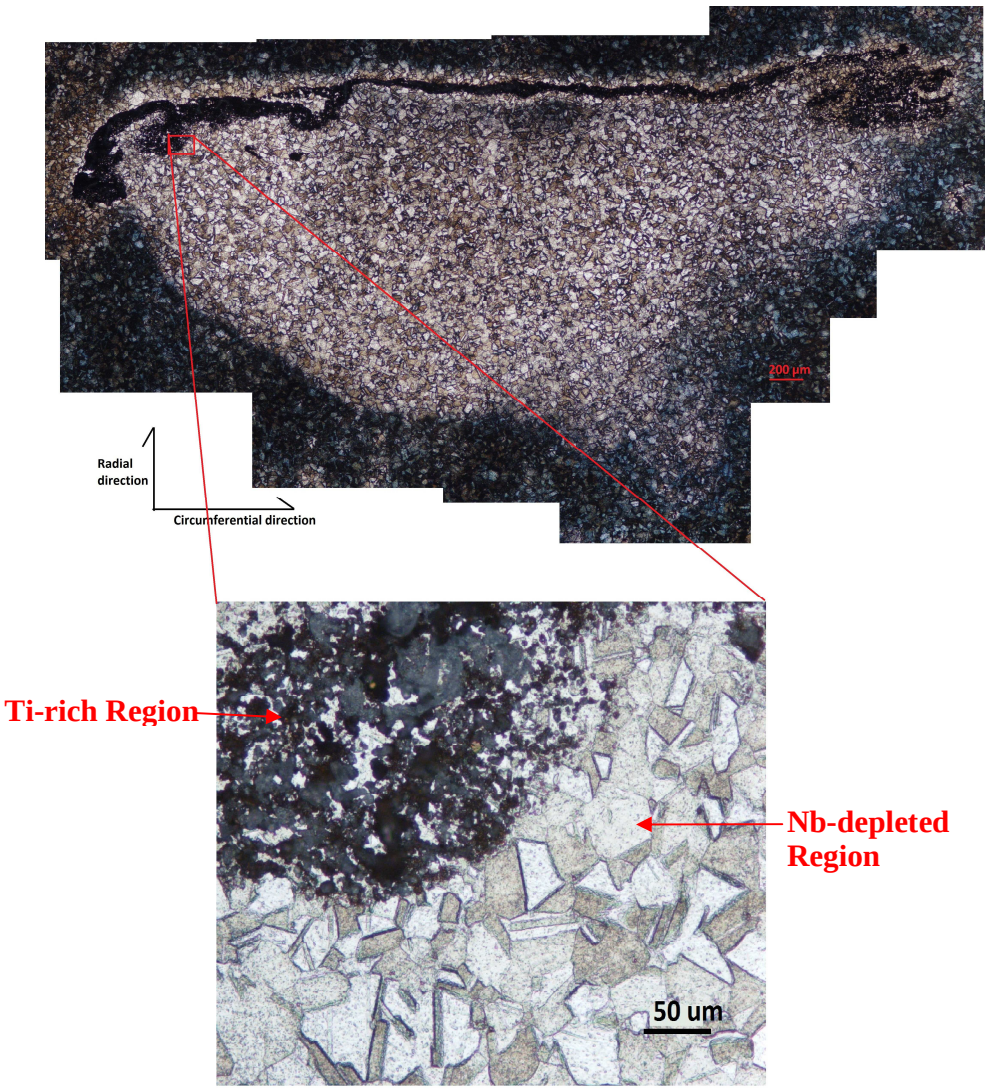

Figure 5.6: An optical image of the Ti-rich region and Nb-depleted region interface.

5.2.2 2-D EDS Images

The Horiba® XGT-7000™ was used to acquire 2-D EDS maps of the Alloy 718 dirty white spot. These images, acquired at sequential depth layers exposed during serial polishing, were used to create a 3-D reconstruction of the Ti-rich region of the dirty white spot. The Nb-depleted region of the white spot was not reconstructed because XRF EDS maps lacked

sufficient contrast in Nb concentration with the bulk material. This is due to the fact that at each point of the XRF EDS map, there are very few X-ray photon counts with which to create an accurate composition spectrum. Essentially, the number of counts is insufficient to determine the difference between the slightly Nb-depleted region and the bulk material. The uncertainty associated with composition quantification is greater than the difference between the Nb-depleted region and the bulk material. See Figure 5.7 for a plot of “sum spectrum” versus “point spectrum” results. A “sum spectrum” is created from 2-D XRF EDS scan data by combining the spectra stored at all locations (pixels) in the map to create one EDS energy spectrum. A “point spectrum” is simply a plot of a spectrum stored for a single pixel of a 2-D XRF EDS map. The low number of counts, about one to two per large peak, in each point spectrum of an XRF EDS map is only adequate to determine if a major element is present or not. There is not enough information at each pixel of the XRF EDS maps to quantitatively determine Nb concentration differences between the Nb-depleted region and the bulk material. A spectrum containing significantly more X-ray photon counts, similar to the sum spectrum in Figure 5.7, is necessary to quantitatively determine such composition differences. This would be possible if one were to acquire a spectrum at each pixel for approximately 100 seconds. Assuming an area of 256 by 256 pixels, acquiring a single 2-D XRF EDS map with quality sufficient for accurate quantification of Nb concentrations would take as much as 77 days. This is an impractical amount of time to spend for a single layer of data for the purposes of serial sectioning.

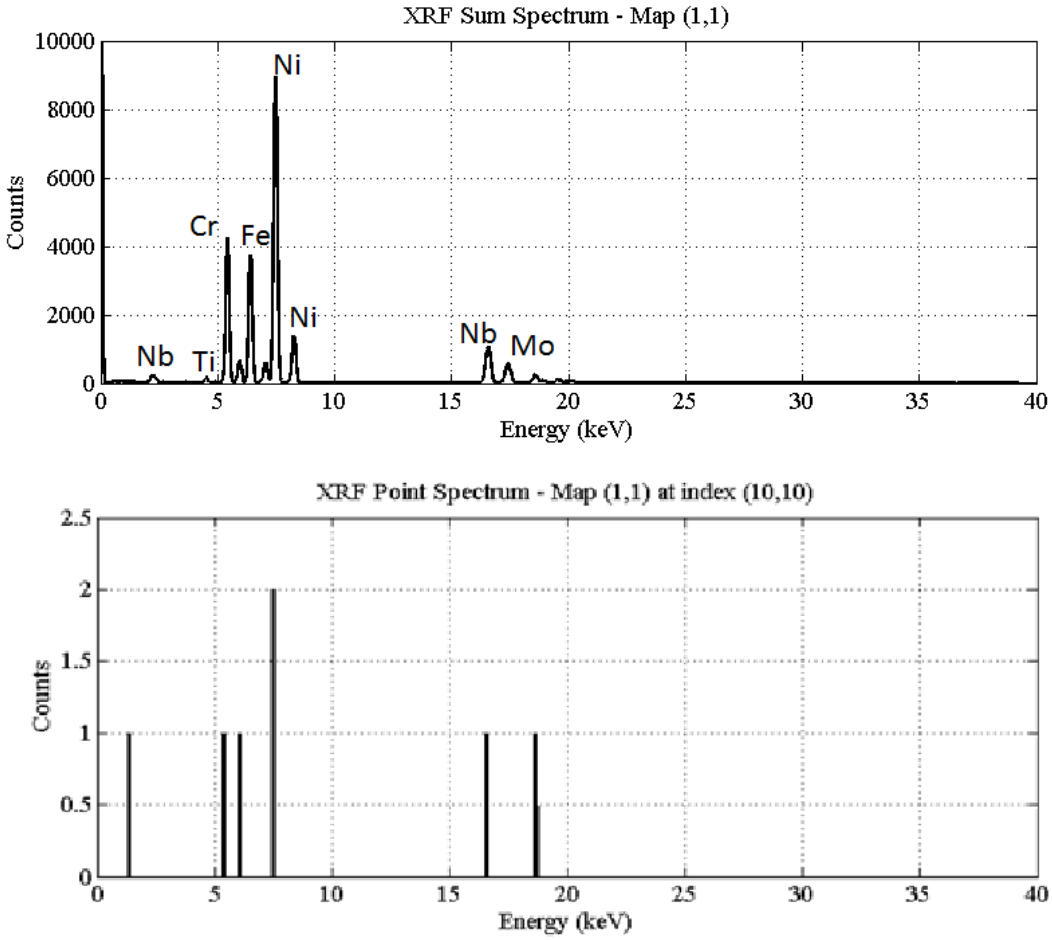

Figure 5.7: An XRF EDS map sum spectrum (top) and a point spectrum (bottom) from the same XRF EDS map.

Figure 5.8 shows an example of a Nb XRF EDS map acquired with the XGT-7000™. This image is a clear example of the inadequacy of the 2-D XRF EDS mapping technique for distinguishing small differences in Nb concentration when using reasonably short scan times of a few hours. In the upper-left frame of the image, the boundary of the Nb-depleted region of the white spot is only somewhat visible. The boundary is lost in the background signal in the other top frames. Figure 5.9 shows an example of a Ti EDS map acquired with the XGT-7000™. In

this map, the Ti-rich region is not lost in the background signal, and there is enough contrast with the signal from the bulk material that the Ti-rich region appears as a clear, discrete anomaly. The variations in intensity between the multiple images used to create the mosaics are caused by normalizing each frame over an area of 256 by 256 pixels with only a few counts at each pixel. Since a fully white pixel indicates a maximum intensity, the frames with a darker appearance may have had a pixel with a maximum intensity of 5 or 6 counts, for example, and the lighter frames may have had a pixel with maximum intensity of 3 or 4 counts.

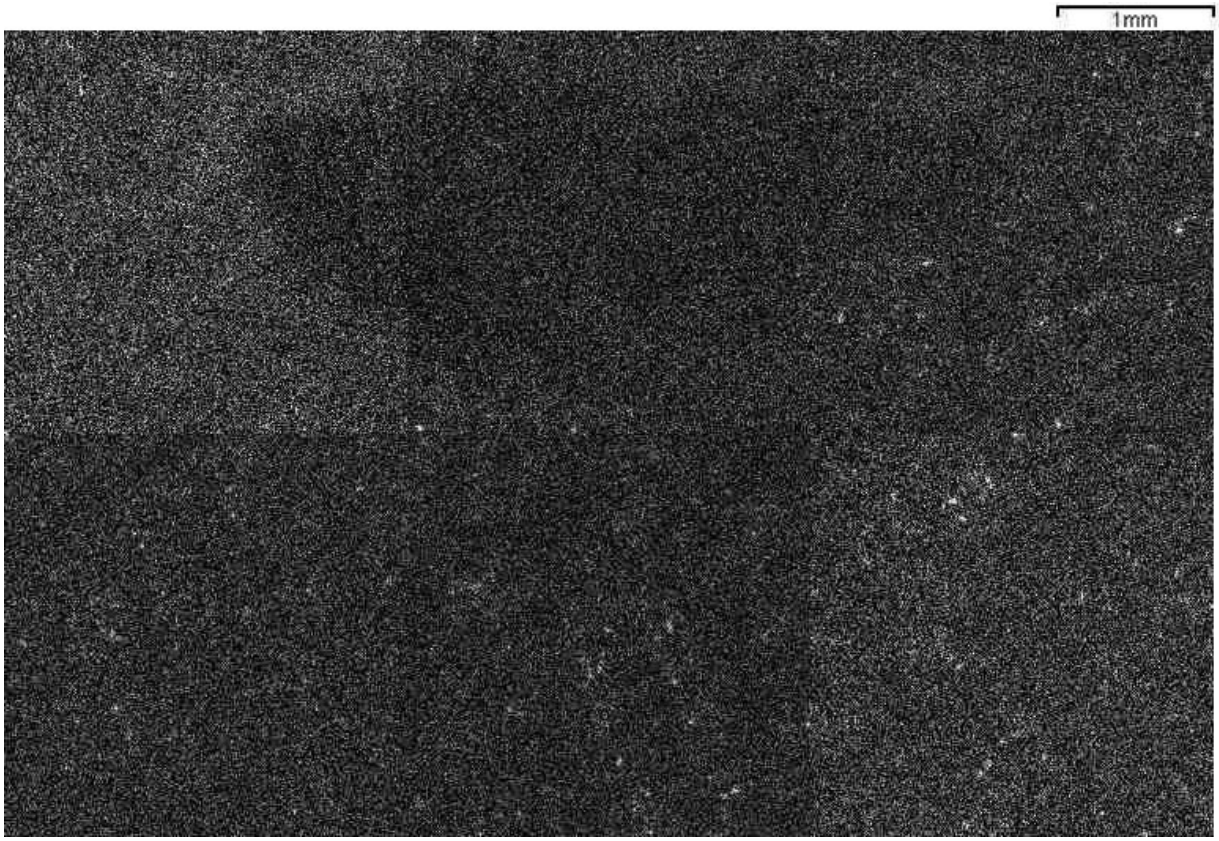

Figure 5.8: An example Nb XRF EDS map from the dirty white spot.

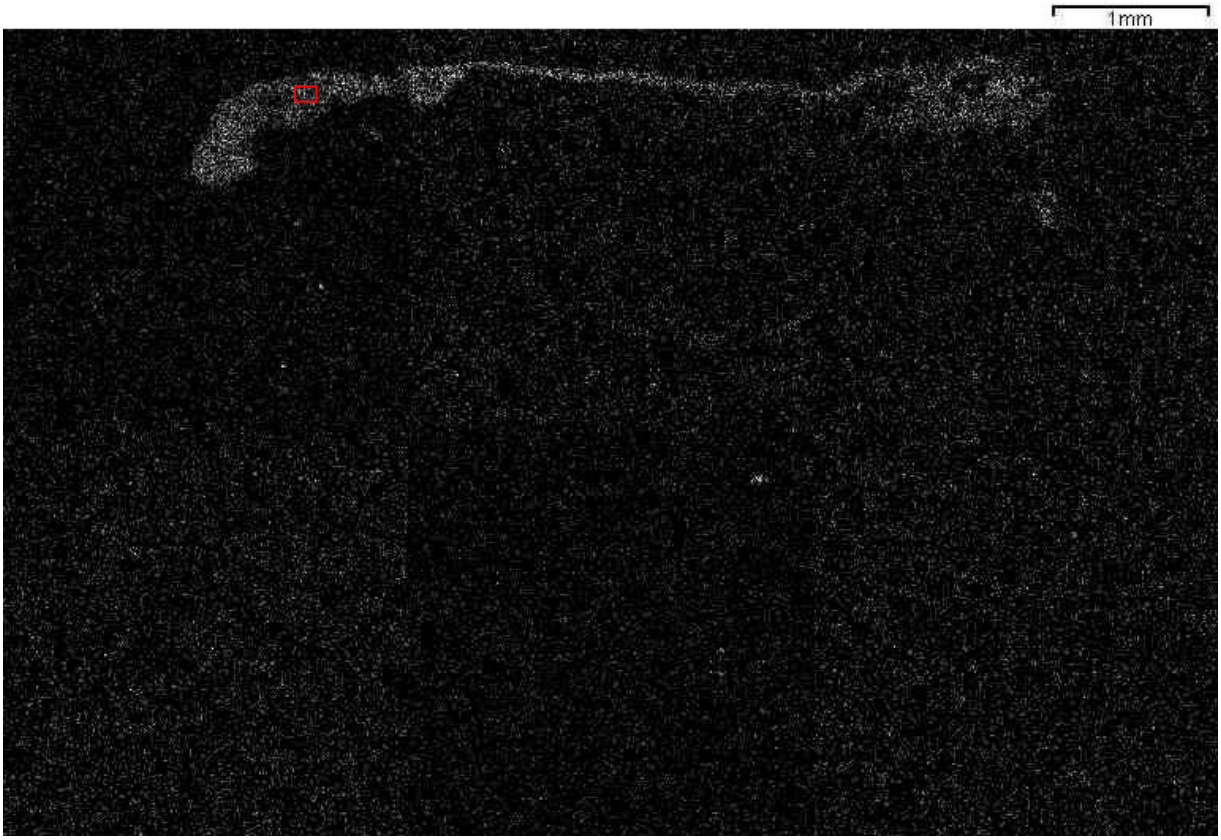

Figure 5.9: An example Ti XRF EDS map from the dirty white spot.

The light element detector on the SEM EDS system is capable of detecting low atomic number elements, such as O and N, and was used to determine their presence in the Ti-rich region of the dirty white spot. Figure 5.10 was acquired from the dirty white spot using the SEM EDS system. The location of Figure 5.10 relative to the white spot is shown by the red square in Figure 5.9. The Ti-rich and N-rich areas of the map overlap each other in the false color image. Oxygen is not present where Ti and N are present. Although the SEM EDS light element detector is able to determine the presence of N and O, it is not sufficient for determining stoichiometry of the Ti-N compounds.

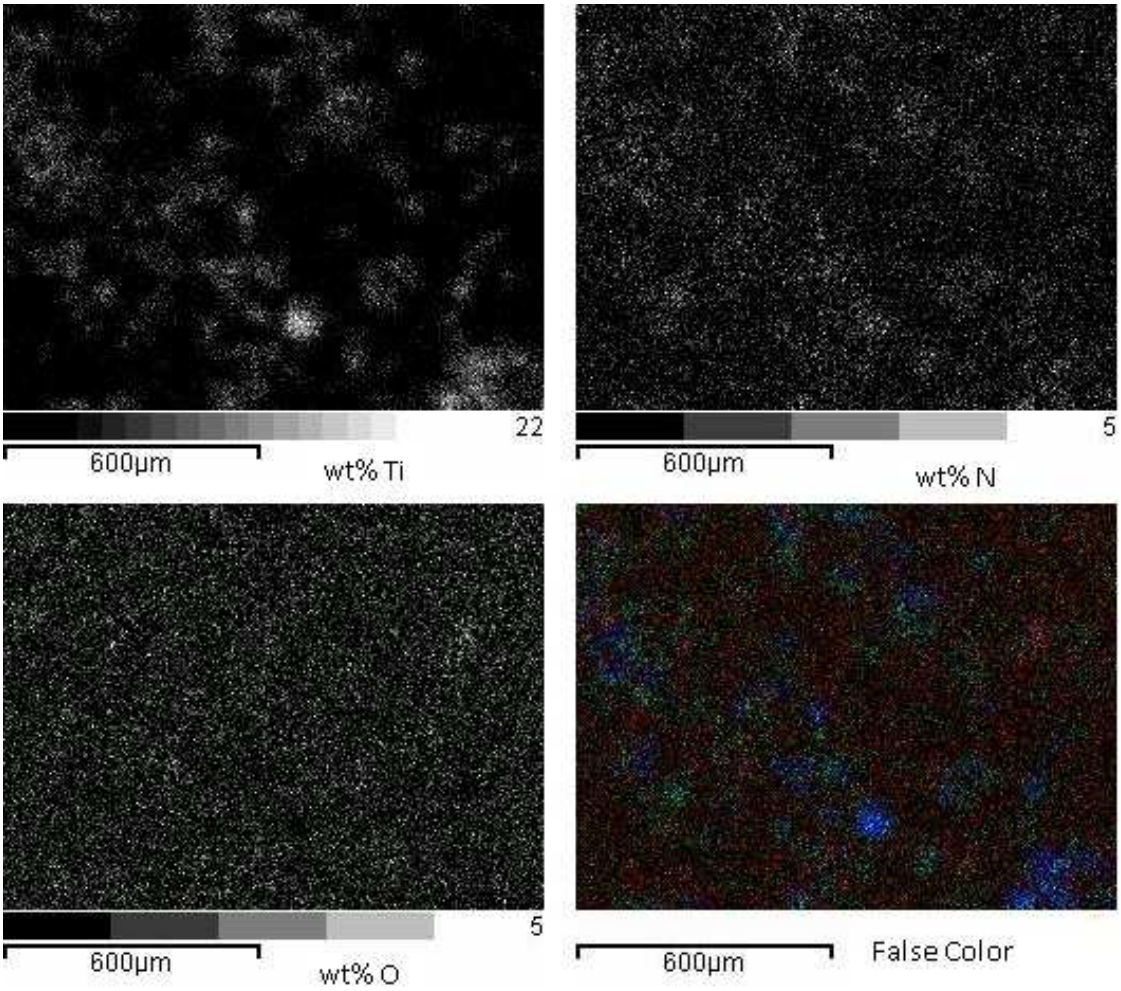

Figure 5.10: SEM EDS element maps of Ti (top left), N (top right), and O (bottom left) and a false color image (bottom right) showing all three elements overlapping. Ti is represented as blue, N as green, and O as red.

5.3 SPOT SCAN COMPOSITION RESULTS

400 µm spot scans were taken of the Ti-rich, Nb-depleted and bulk regions on multiple layers of the specimen using the XRF EDS system. The results were then quantified using the XGT-7000™ software. The composition values from the same region of in all layers were averaged to produce an average value of the composition for each of the three different regions

in the Alloy 718 specimen. Composition values from the XRF EDS analysis were plotted versus layer depth to determine any composition changes with depth into the specimen. In order to determine any composition changes across the polishing surface, 10 µm spot scans were taken across the radial and circumferential directions of one layer, see Figure 4.2, in the Ti-rich and Nb-depleted regions. 10 µm spot scans were also taken across the circumferential direction of the Nb-depleted region to determine any composition changes in this direction.

5.3.1 XRF EDS Region Averages

Figure 5.11 shows a schematic of the two different regions of the dirty white spot. The approximate locations of the 400 µm spot scans taken on each layer are shown.

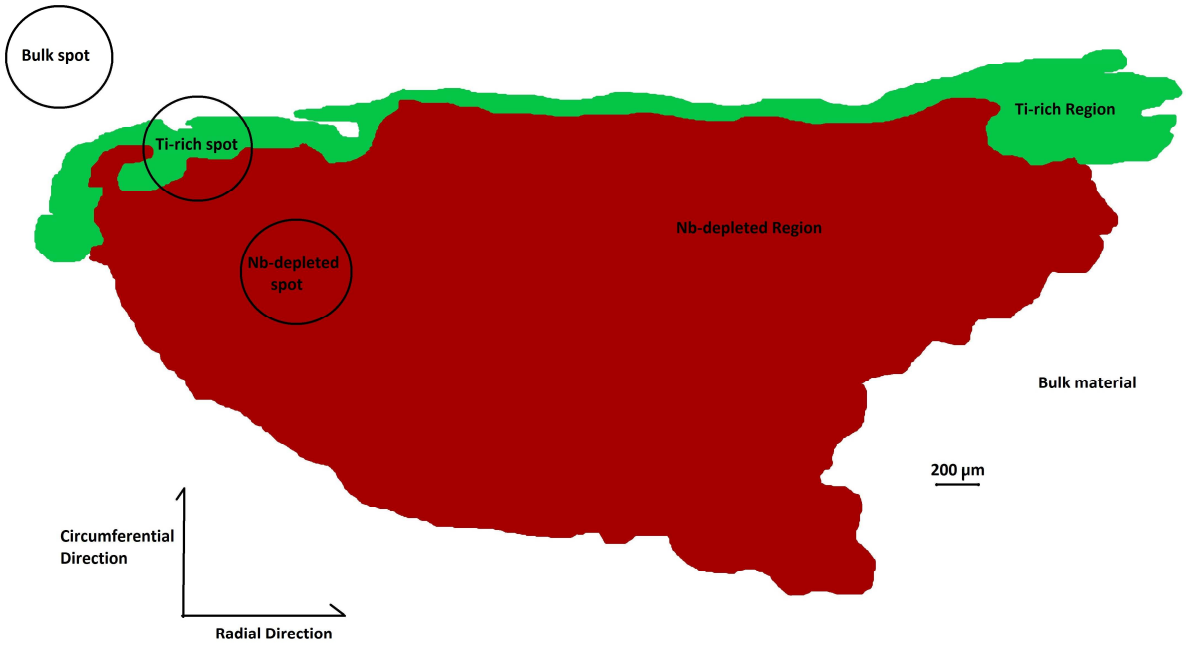

Figure 5.11: Locations of XRF EDS 400 µm spot scans.

Table 5.1 shows average quantification results from six layers of 400 µm XRF EDS spot scans as a percent difference from the bulk Alloy 718 material. These results show that the Nb-depleted region of the dirty white spot is depleted in Nb by 24%. It is necessary to note that the Ti-rich region of the dirty white spot was less than 400 µm wide, which was the spot size used to collect these data. As a result, the spectra used to create the results for the Ti-rich region in Table 5.1 necessarily include some signal from both the Nb-depleted region and bulk region of the Alloy 718 specimen. Thus, it is safe to assume that the Ti-rich region is actually enriched in Ti more than 400% from the bulk material as shown in Table 5.1.

Table 5.1: 400 µm XRF EDS Spot Scan Quantification Results, Averaged Over Multiple Layers of Data

	% Difference, by weight, in Composition from Bulk Material	
	Region	
Element	Nb-Depleted	Ti-Rich
Al	17%	28%
Si	-14%	-21%
Ti	-15%	400%
Cr	2%	-3%
Mn	14%	-8%
Fe	4%	-4%
Co	-9%	-10%
Ni	1%	-5%
Nb	-24%	0%
Mo	-4%	-4%

5.3.2 XRF EDS Spatial Composition Variations

Measurement uncertainties for the 400 µm spot scans were calculated using the following method. See Equations 5.1-3 [29]. *A* in Equation (5.1) represents the percent difference in concentration, by weight, of a particular element *X* at a specific location relative to the concentration of element *X* in the bulk material. *A* is a function of *B* and *C*. *B* represents the wt% concentration of element *X* at a specific location. *C* represents the wt% concentration of element *X* in the bulk material. The variation in *A*, *dA*, due to variations in *B* and *C* can be calculated by taking the absolute derivative of *A*, as shown in Equation (5.2). The partial derivatives ($\partial A/\partial B$) and ($\partial A/\partial C$) in Equation (5.2) are sensitivity factors related to how the value of *A* varies relative to variations in *B* and *C*. These can be calculated directly from the derivative of Equation (5.1). The values *dB* and *dC* are the uncertainties of *B* and *C*. These values are assumed equal to the 3σ (three times the standard deviation) values for the elements being analyzed. The 3σ values are provided by the XRF EDS software for each element in each scan. The 3σ value represents a 99.7% confidence interval for the reported element concentration. The 3σ values are calculated by the XRF EDS software using the following: capillary size, scan time, scan conditions, and reference standard information. The magnitude of the variation in *A* can be calculated using the root-sum-squares (RSS) method, which is equivalent to the equation for the magnitude of a vector, see Equation (5.3) [29]. Uncertainty of the reported Nb depletion in the Nb-depleted region versus the bulk material, in wt% difference, was calculated to be approximately 1 to 2%. Uncertainty of the reported Ti enrichment in the Ti-rich region versus the bulk material, in wt% difference, was calculated to be approximately 20 to 25%.

$$A = A(B,C) = \frac{B-C}{C} \qquad \text{Equation (5.1)}$$

$$dA = \left(\frac{\partial A}{\partial B}\right)\Big|_C dB + \left(\frac{\partial A}{\partial C}\right)\Big|_B dC \qquad \text{Equation (5.2)}$$

$$\|dA\| = \sqrt{\left[\left(\frac{\partial A}{\partial B}\right)dB\right]^2 + \left[\left(\frac{\partial A}{\partial C}\right)dC\right]^2} \qquad \text{Equation (5.3)}$$

where A = % difference

B = wt% value of Ti/Nb from Ti/Nb scan,

C = wt% value of Ti/Nb from bulk scan,

dA = error of % difference calculation,

dB = 3σ value of Ti/Nb concentration from Ti/Nb scan,

and dC = 3σ value of Ti/Nb concentration from bulk scan.

Figures 5.12 and 5.13 present XRF EDS 400 µm spot scan compositional quantification results as percent difference in concentration, by weight, compared to the bulk material versus depth polished for the Nb-depleted and Ti-rich regions of the dirty white spot, respectively. These data are from the same set used to calculate the average compositions shown in Table 5.1. For the Nb-depleted region, the variations in composition show no clear trend, but are significant relative to measurement uncertainties. For the Ti-rich region, the variations in composition are within the range of measurement uncertainty, with the exception only of the measurement at the deepest layer.

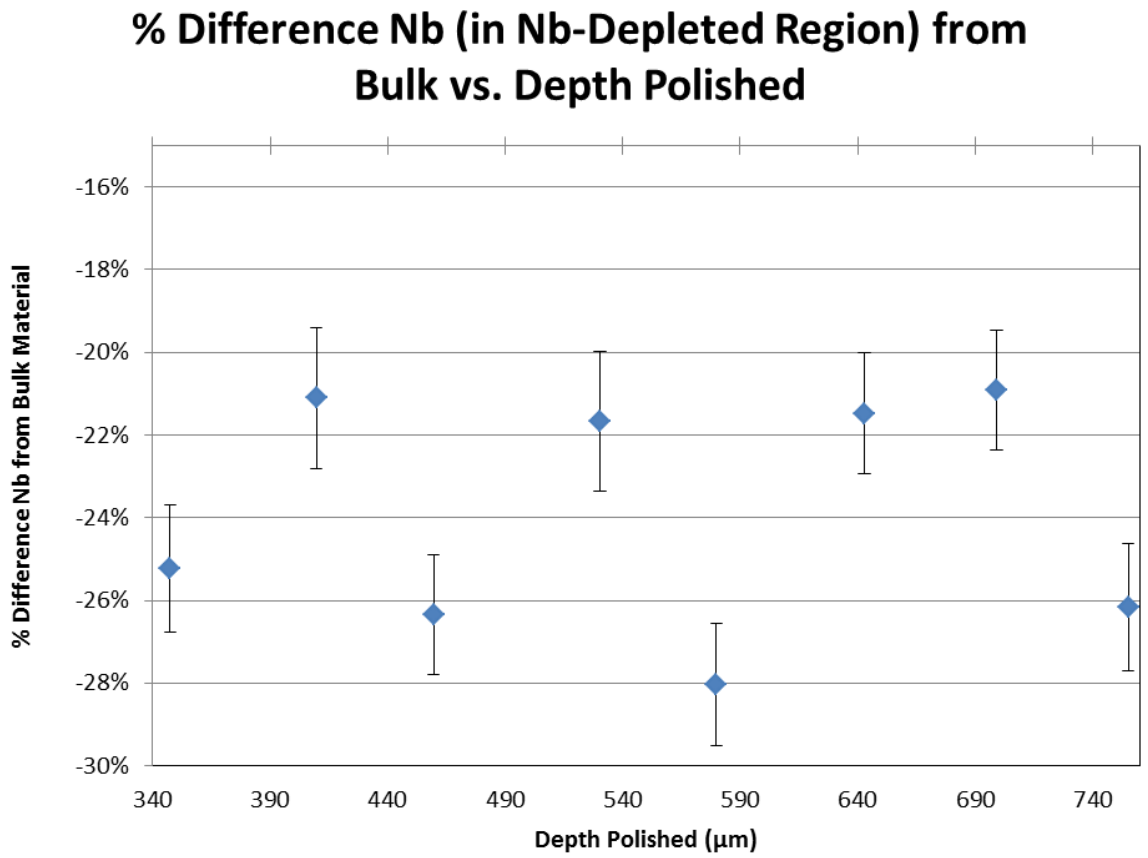

Figure 5.12: A plot of percent difference Nb composition, by weight, in the Nb-depleted region from the bulk Alloy 718 material vs. depth polished, as indicated by XRF EDS 400 µm spot scans.

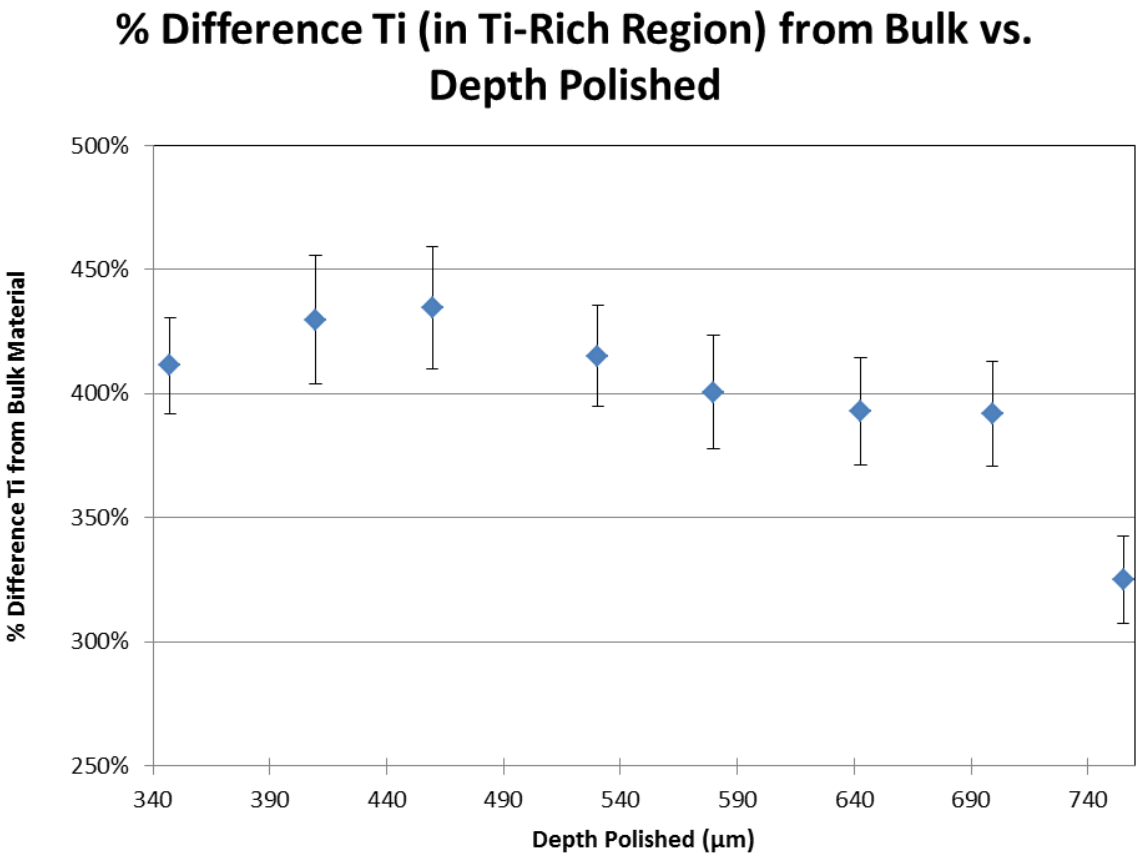

Figure 5.13: A plot of percent difference Ti composition, by weight, in the Ti-rich region from the bulk Alloy 718 material vs. depth polished, as indicated by XRF EDS 400 µm spot scans.

Figure 5.14 shows a schematic of the locations of five different XRF EDS 10µm spot scans used to determine composition across the dirty white spot.

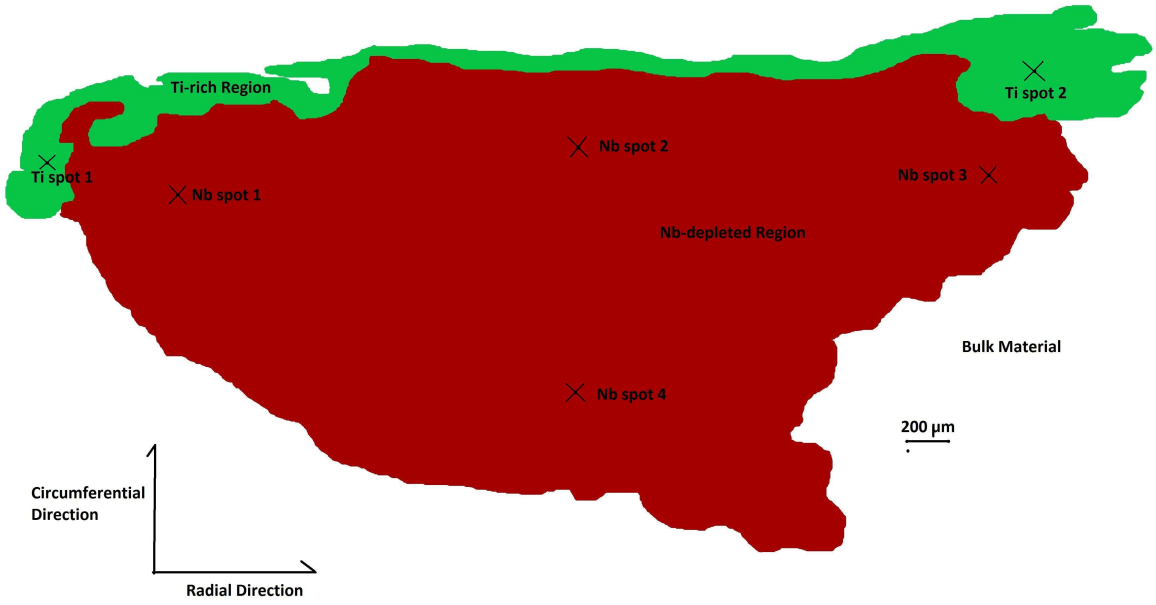

Figure 5.14: A diagram of the dirty white spot, showing 10 µm spot scan locations.

Table 5.2 provides XRF EDS composition quantification results from the 10 µm spot scans shown in Figure 5.14, as percentage differences from the bulk material. These results show that there is a decrease in Ti enrichment along the radial direction of the white spot. There is also a slight increase in Nb concentration along the radial direction. There is a decrease in Nb concentration along the circumferential direction.

Table 5.2: 10 µm XRF EDS Spot Scan Quantification Results, for determining compositional trends across specimen polishing surface

Spot	Ti Spot 1	Ti Spot 2	Nb Spot 1	Nb Spot 2	Nb Spot 3	Nb Spot 4
% Difference in composition from bulk material	1348%	607%	-37%	-35%	-24%	-28%

5.4 3-D RECONSTRUCTION

A 3-D reconstruction of the Ti-rich region of the dirty white spot was created using segmented composite XRF EDS images from each layer of data and the Reconstruct© software package. Note that the Ti-rich region is actually composed of many discrete Ti-N particles, with sizes on the order of approximately 3 µm. Representing the Ti-rich region as a single object only represents the macroscopic morphology of the enriched region, not the individual particles that give the region its characteristics. The Nb-depleted region was not reconstructed in 3-D due to a lack of contrast between the Nb-depleted and bulk regions in the XRF EDS map data. Figures 5.15 and 5.16 show two different views of the 3-D reconstruction of the Ti-rich region in the Alloy 718 dirty white spot.

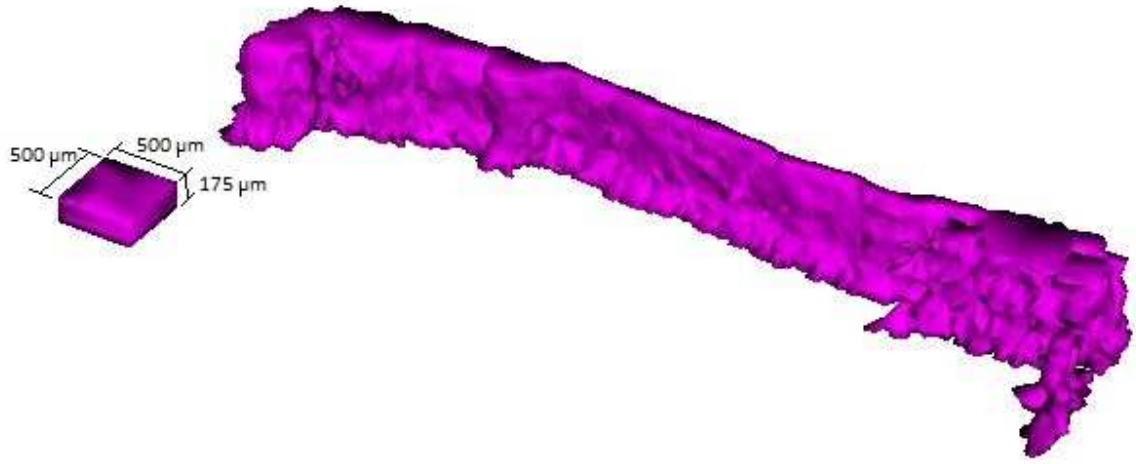

Figure 5.15: A 3-D reconstruction of the Ti-rich region, view 1.

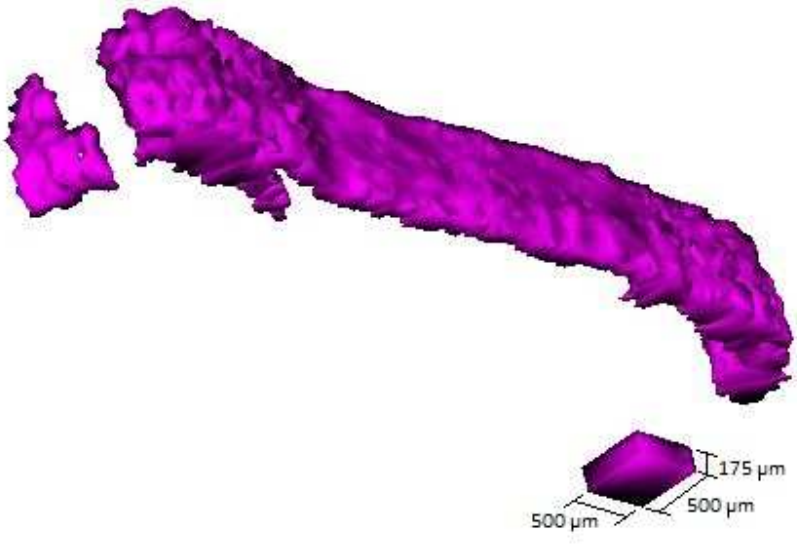

Figure 5.16: A 3-D reconstruction of the Ti-rich region, view 2.

Chapter 6: Discussion

6.1 DISCUSSION

Chapter 5 presented 3-D characterization of composition and morphology of a dirty white spot in an Alloy 718 specimen. This particular dirty white spot contains a Nb-depleted region and a Ti-enriched region "capping" the Nb-depleted region. Figures 5.2, 5.5, and 5.7 show that the Ti-enriched region of the dirty white spot comes into direct contact with the Nb-depleted region.

XRF EDS data show that the main difference between the Ti-rich region and the bulk Alloy 718 material is the presence of an increased amount of Ti. The enrichment in Ti varies anywhere from 600% to 1400% compared to the bulk Alloy 718 material, according to 10 µm spot scans. The Ti enrichment decreases along the radial direction, see Figure 4.2, relative to the original ingot. See Figure 5.14 and Table 5.2 for supporting. Ti concentration does not significantly vary with depth in the Ti-rich region, see Figure 5.13. Uncertainty in percent difference, by weight, of Ti in the Ti-rich region relative to the bulk material, using 400 µm capillary XRF EDS spot scans, is approximately ±20 to 25%. BSE images from the SEM show the microstructure of the Ti-rich region to be composed of discrete particles dispersed in a matrix of Alloy 718 bulk material. These discrete particles are approximately 0.5 µm to 3 µm in diameter, see Figures 5.3 and 5.4. 2-D SEM EDS composition maps show the discrete particles in the Ti-rich region to be composed of Ti and N. See Figure 5.11 for an image of this SEM EDS analysis. The slightly golden hue of the unetched Ti-rich region in Figure 5.1 supports the conclusion that the particles in the Ti-rich region are Ti-N compounds, most likely TiN. In addition, there is a lack of O present in the areas containing Ti. This further suggests that the Ti

particles are nitrides, not oxides. The macrostructure of the Ti-rich region in 3-D is shown in Figures 5.15 through 5.16. These figures show that the XRF EDS serial sectioning technique outlined in Chapter 2 is adequate for creating a 3-D representation of anomalies in Alloy 718 that have a composition significantly different from the bulk material. Figure 5.10 shows an example of an XRF EDS map that was segmented and used in creating a 3-D reconstruction of the Ti-rich region. The Ti-rich region clearly changes shape with depth. It is important to note that the actual microstructure of the Ti-rich region, consisting of discrete particles less than 5 µm in diameter, is not represented by the 3-D reconstruction of XRF EDS data. However, the reconstruction accurately represents the shape of the Ti-rich region on a scale of approximately 20 µm or larger.

XRF EDS data show that the main difference between the Nb-depleted region and the bulk Alloy 718 material is a lower concentration of Nb. The Nb concentration in the white spot is approximately 24% less than in the bulk Alloy 718 material, according to averages of 400 µm capillary XRF EDS spot scans from six layers, see Table 5.1. See Figure 5.12 for locations of these scans. The concentration of Nb in the white spot varies with location. The Nb depletion decreases from 37% to 24% along the radial direction in the white spot. The Nb depletion increases from 28 % to 35% along the circumferential direction, see Figure 5.14 and Table 5.2. Nb concentration varies with depth, although there is no clear trend in this variation, see Figure 5.13. Uncertainty in percent difference, by weight, of Nb in the Nb-depleted region relative to the bulk material, using 400 µm capillary XRF EDS spot scans, is approximately ±2%. Optical images of the Nb-depleted region and bulk material interface show that no dendritic structure is present in the microstructure of the Nb-depleted region, which could be expected if the white spot originated from fall-in from the melting VAR electrode. However, remaining dendritic structure could have been eliminated by recrystallization during the forging process. Lineal intercept grain size measurements show the average grain size in the Nb-depleted region of the

white spot and bulk material to be 24 µm and 25 µm, respectively. This is not a significant difference and suggests that the white spot is unlikely to have had a coarse, dendritic microstructure, significantly different from the bulk material, prior to forging and any recrystallization. The XRF EDS serial sectioning and 3-D reconstruction technique were not adequate for creating a 3-D representation of the Nb-depleted region macrostructure. This is because of very low count numbers present at each pixel in the 2-D XRF EDS maps, and only a slight difference in Nb concentration between the bulk material and the Nb-depleted region. See Figure 5.8 for an illustration of the low count numbers present at an individual pixel of a 2-D XRF EDS Nb-depleted region map. This results in little contrast between the two regions present in Figure 5.9. With only 1 to 2 counts per major peak, it is impossible to determine quantitative amounts of elements present. Instead, it is only possible to determine whether or not the element is present. Although the 2-D XRF EDS mapping technique was not useful for 3-D reconstructions of the Nb-depleted region, it is important to note that the XRF equipment is fully capable of detecting the slight concentration differences by using longer spot scans, which result in many more X-ray photon counts.

The presence of TiN particles in the Ti-rich region, as well as the non-dendritic nature of the dirty white spot, indicate that the dirty white spot likely originated in the crown or shelf region of the solidifying VAR ingot. The crown and shelf regions are expected to contain Alloy 718 with a lower Nb content, as well as nitride and oxide compounds [4]. The TiN particles might have formed a cap on the crown or shelf. Perturbations of the melt pool or arc instability may have caused a piece of the crown or shelf to fall into the melt pool. The Nb concentration in the Ti-rich region of the dirty white spot is the same as the bulk material, indicating that the material between the Ti-N particles is the same as the bulk material. This, along with the size of the discrete Ti-N particles (0.5 to 3 µm in diameter), could indicate that the region was initially

porous and was penetrated by the melt after falling from the crown and/or shelf regions. The material that fell into the melt pool was likely trapped in the solidifying mushy zone before completely melting, causing it to become the observed dirty white spot.

Overall, these results confirm that the XRF EDS serial sectioning method of 3-D compositional data collection useful for characterization of superalloy anomalies. It is possible to detect variations in composition on the order of approximately 1.0 wt% with the available equipment, which means that reliable information about composition gradients in 3-D can be collected. The Reconstruct© method of representing 3-D XRF EDS data is limited to data in which discrete boundaries can be determined by large contrast difference in the data. This technique is useful for representing macroscopic features with large concentration differences, such as the Ti-enriched region of the dirty white spot.

Chapter 7: Conclusions

7.1 CONCLUSIONS

An Alloy 718 specimen containing a dirty white spot was obtained from a commercial supplier and was studied using serial polishing techniques. A set of 3-D XRF EDS data was acquired from the dirty white spot by serial polishing and application of 2-D XRF EDS analysis at each polish depth (layer). The resulting series of 2-D EDS maps were segmented, where possible, and then stacked to create a 3-D representation of the dirty white spot. In addition, XRF EDS spot scans were performed across multiple layers for accurate compositional quantification at specific locations. SEM and optical microscopy techniques were used to further characterize the dirty white spot. The following conclusions are made from this study:

- The dirty white spot consists of adjacent Ti-rich and Nb-depleted regions. The Ti-rich region "caps" one side of the Nb-depleted region.

- Composition of the dirty white spot varies along the radial direction of the ingot. Ti-enrichment decreases from 1400% to 600%, by weight, relative to the bulk material, along the radial direction. Nb-depletion decreases from 37% to 24%, by weight, relative to the bulk material, along the radial direction.

- There is a slight composition variation along the circumferential direction in the Nb-depleted region of the dirty white spot. Levels of Nb-depletion vary from 28% to 35%, by weight, compared to the bulk material, along the circumferential direction of the ingot.

- There are variations of Nb composition in the vertical direction of the ingot over the depth polished; however, the variation follows no clear trend. There is no composition variation of Ti in the white spot along the vertical direction in the ingot, except for one measurement at the greatest depth.

- BSE SEM images of the Ti-rich region show that it contains discrete particles with diameters ranging from 0.5 µm to 3µm. These particles appear to be dispersed in a matrix of bulk Alloy 718 material.

- SEM EDS maps of the Ti-rich region show overlap of Ti and N. This indicates that the discrete particles are a Ti-N compound. The golden hue of the Ti-rich region in optical microscope images suggests that the Ti-N compound is TiN, which typically has a gold color. There is a lack of O present in the areas containing Ti, which suggests the Ti particles are nitrides, not oxides.

- The presence of N and O in the Ti-rich region suggests that the dirty white spot was produced by a fall-in from the crown or shelf region of the solidifying VAR ingot, where oxides and nitrides are more common.

- Nb concentrations in the Ti-rich and bulk regions are the same. This indicates that the bulk region and material between Ti-N particles are the same. Because of this, it is possible that the Ti-rich region of the fall-in was a porous and was penetrated by the melt.

- The non-dendritic structure of the dirty white spot suggests that it is fall-in from the crown or shelf region of the solidifying VAR ingot, rather than fall-in from an electrode cavity. If the dirty white spot originated from the electrode, a coarse dendritic structure

would be expected. It is possible that the dendritic structure would be eliminated by recrystallization during the forging process. Lineal intercept grain size measurements reveal the grain sizes in the Nb-depleted and bulk regions to be similar (24 µm and 25 µm, respectively). The similar grain sizes suggest similar microstructures prior to any recrystallization, which makes it unlikely for the white spot to have had the coarse dendritic structure typical of electrode fall-in prior to forging.

- The 3-D reconstruction method is adequate for reconstructing areas with large composition differences from the bulk material, such as the Ti-rich region. The resolution of such reconstructions is limited by the resolution of the data sets used in their generation.

- The 3-D reconstruction method is not useful for low-contrast data sets, such as XRF EDS map scans of the Nb-depleted region in this study. This is due to very low count levels for Nb in the XRF EDS 2-D maps.

- It would be necessary to acquire a significantly larger number of X-ray photon counts for 2-D XRF EDS maps, which would require much longer scan times, to achieve contrast great enough to segment data for the Nb-depleted region.

7.2 SUGGESTIONS FOR FUTURE WORK

It would be desirable to have a piece of the crown and shelf region of a solidifying VAR ingot for compositional characterization. This would allow for the direct comparison of elemental concentrations in the crown and shelf regions to the elemental concentrations in the Ti-rich region of the dirty white spot. Such a comparison would be useful to test the hypothesis that

the dirty white spot is produced by fall-in from one of these regions. In addition, further light-element analysis of the Ti-rich region would be valuable to determine the exact N and O amounts and compounds present. Possible light-element characterization techniques would include wavelength dispersive spectroscopy (WDS), inert gas fusion analysis, and inductively coupled plasma atomic emission spectroscopy [27, 28].

Additional polishing and feature reconstruction over a much larger depth would also be desirable. Studying a larger depth, ideally until the white spot was no longer present, would give a better 3-D representation of the white spot's morphology, as well as the relationship between the Ti-rich and Nb-depleted regions. This analysis could also provide more support for the idea that the dirty white spot underwent partial melting.

Finally, the creation of a software suite designed specifically for the visualization of 3-D compositional data sets is needed. Software that combines the data indexing and quantification routines of the XRF EDS software, the capability to merge multiple 2-D maps together, and 3-D visualization techniques is essential for a better understanding of the information stored within the large 3-D data sets acquired with the serial polishing technique. A method of merging low-magnification EDS data sets, like those collected with the XRF EDS system, with high-magnification EDS data sets, like those collected with the SEM EDS system, would also be valuable for the 3-D characterization procedure.

References

[1] Reed, R.C., 2006, *The Superalloys, Fundamentals and Applications*, Cambridge University Press, New York, pp. 222-227, Chap. 4

[2] ASM International, 2002, *Inconel 718,* Engineering Alloys Digest Inc., Upper Montclair, New Jersey, pp. 1-2

[3] Mitchell, A., Kawakami, A., Cockcroft, S.L., 2006, "Beta Fleck and Segregation in Titanium Alloy Ingots," *High Temperature Materials and Processes,* **25**, (5-6), pp. 337-349

[4] Jackman, L.A., Maurer, G.E., Widge, S., 1994, "White Spots in Superalloys," *Proceedings of the International Symposium on Superalloys,* Minerals, Metals, and Materials Society, Warrendale, PA, pp. 153-165

[5] Zanner, F., Williamson, R., Erdmann, R., 2005, "On the Origin of Defects in VAR Ingots," *Proceedings of the Liquid Metals Processing Consortium*, ASM International, pp. 13-27

[6] Morita, K., Suzuki, T., Taketsuru, T., Evans, D.G., Yang, W., 2001, "The Tendency for Freckle Formation in Alloy 718," *Proceedings of the International Symposium on Superalloys and Various Derivatives*, The Minerals, Metals, and Materials Society, Warrendale, PA, **1,** pp. 149-160

[7] Brooks, J.A., Kraficik, J.S., Schneider, J.A., VanDenAvyle, J.A., "Fe Segregation in Ti-10V -2Fe-3Al 30 Inch VAR Ingot B-Fleck Formation," Sandia National Laboratories, CA

[8] Zagrebelnyy, D., Krane, J.M., 2008, "Segregation Development in Multiple Melt Vacuum Arc Remelting," *Metallurgical and Materials Transactions*, **40**, (3), pp.281-288

[9] Soller, A., Jardy, A., Larue, R., Ablitzer, D., 2005, "Behaviour of Discrete White Spot Precursors in a VAR Liquid Pool," *Proceedings of the 2005 International Symposium on Liquid Metal Processing and Casting,* ASM International, pp. 39-48

[10] Mitchell, A., 1986, "White Spot Defects in VAR Superalloys," *High Temperature Alloys for Gas Turbines and Other Applications,* D. Reidel Publishing, Dordrecht, Netherlands, **1**, pp. 679-696

[11] Shved, F., 2009, "On the Origin of the White Spot Defect in Vacuum Arc Remelted Ingots," *International Symposium on Liquid Metal Processing and Casting,* The Minerals, Metals, and Materials Society, Warrendale, PA, pp.85-93

[12] Erdeljac, J.P., Henein, H., Mitchell, A., 1985, "Melting Kinetics of Segregated Particles in VAR 718," *Transactions of the Iron and Steel Society of AIME*, **6**, pp.51-63

[13] Malara, C., Radavich, J., 2005, "Alloy 718 Large Ingots Studies," *Proceedings of the International Symposium on Superalloys and Various Derivatives,* The Minerals, Metals, and Materials Society, Warrendale, PA, pp. 25-33

[14] Chang, J.K., Taleff, E.M., Krajewski, P.E., 2009, "Effect of Microstructure on Cavitation during Hot Deformation of a Fine-Grained Aluminum-Magnesium Alloy as Revealed through Three-Dimensional Characterization," The Minerals, Metals, and Materials Society, Warrendale, PA, **40A,** pp. 1-3

[15] Fiala, J.C., 2005, *Journal of Microscopy*, **218**, pp. 52-61

[16] *X-Ray Analytical Microscope XGT-7000V Instruction Manual*, 2007, Horiba Ltd., Kyoto, Japan

[17] *Allied High Tech Products, Inc. Multiprep™ System,* 2004, Allied High Tech Inc., Rancho Dominguez, CA

[18] Jenkins, R., 1999, *X-Ray Fluorescence Spectrometry,* John Wiley & Sons, New York, pp. 8-

11, Chap. 1
[19] *Inconel® Alloy 718*, 2007, Special Metals Corporation, New Hartford, New York
[20] *X-Ray Mass Attenuation Coefficients*, 1996, National Institute of Standards and Technology, Gaithersburg, Maryland
[21] *JSM-5610 Scanning Electron Microscope*, 2001, JEOL Ltd., Tokyo, Japan
[22] *Nikon Epiphot 300/200*, 2004, Nikon Corporation, Yokohama, Japan
[23] *Certificate of Analyses*, 2010, Geller Microanalytical Laboratory, Topsfield, MA
[24] James, A.M., Lord, M.P., *Macmillan's Chemical and Physical Data*, Macmillan, London, United Kingdom
[25] Goldstein, J., Newbury, D., 2003, *Scanning Electron Microscopy and X-Ray Microanalysis*, Springer Science, New York, pp. 292-295, Chap. 6
[26] Evans, D., 2011, Engineer at Special Metals Corporation, private communication
[27] Davis, J.R., 1998, *Metals Handbook Desk Edition*, ASM International
[28] Mills, K., Davis, J.R., 1986, *Metals Handbook*, ASM International, **10**
[29] Figliola, R.S., Beasley, D.E., 1995, *Theory and Design for Mechanical Measurements*, John Wiley and Sons, Inc., New York, pp. 177-181, Chap. 5
[30] ASTM Standard E112, 2010, "Standard Test Methods for Determining Average Grain Size," ASTM International, West Conshohocken, PA, 2010, DOI: 10.1520/E0112-10, www.astm.org